Author/s:
Almeida, CF;Gully, BS;Jones, CM;Kedzierski, L;Gunasinghe, SD;Rice, MT;Berry, R;Gherardin, NA;Nguyen, TT;Mok, YF;Reijneveld, JF;Moody, DB;Van Rhijn, I;La Gruta, NL;Uldrich, AP;Rossjohn, J;Godfrey, DI

Title:
Direct recognition of an intact foreign protein by an αβ T cell receptor

Date:
2024-12-01

Citation:
Almeida, C. F., Gully, B. S., Jones, C. M., Kedzierski, L., Gunasinghe, S. D., Rice, M. T., Berry, R., Gherardin, N. A., Nguyen, T. T., Mok, Y. F., Reijneveld, J. F., Moody, D. B., Van Rhijn, I., La Gruta, N. L., Uldrich, A. P., Rossjohn, J. & Godfrey, D. I. (2024). Direct recognition of an intact foreign protein by an αβ T cell receptor. Nature Communications, 15 (1), pp.8816-. https://doi.org/10.1038/s41467-024-51897-3.

Persistent Link:
https://hdl.handle.net/11343/358869

nature communications

Article

https://doi.org/10.1038/s41467-024-51897-3

Direct recognition of an intact foreign protein by an αβ T cell receptor

Received: 19 December 2021

Accepted: 21 August 2024

Published online: 11 October 2024

Check for updates

Catarina F. Almeida[1,10], Benjamin S. Gully[2,10], Claerwen M. Jones[2], Lukasz Kedzierski[2,9], Sachith D. Gunasinghe[2,3], Michael T. Rice[2], Richard Berry[2], Nicholas A. Gherardin[1], Trang T. Nguyen[2], Yee-Foong Mok[4], Josephine F. Reijneveld[5,6,7], D. Branch Moody[5], Ildiko Van Rhijn[5,6], Nicole L. La Gruta[2], Adam P. Uldrich[1,11] ✉, Jamie Rossjohn[2,8,11] ✉ & Dale I. Godfrey[1,11] ✉

αβ T cell receptors (αβTCRs) co-recognise antigens when bound to Major Histocompatibility Complex (MHC) or MHC class I-like molecules. Additionally, some αβTCRs can bind non-MHC molecules, but how much intact antigen reactivities are achieved remains unknown. Here, we identify an αβ T cell clone that directly recognises the intact foreign protein, R-phycoerythrin (PE), a multimeric $(\alpha\beta)_6\gamma$ protein complex. This direct αβTCR–PE interaction occurs in an MHC-independent manner, yet triggers T cell activation and bound PE with an affinity comparable to αβTCR–peptide–MHC interactions. The crystal structure reveals how six αβTCR molecules simultaneously engage the PE hexamer, mediated by the complementarity-determining regions (CDRs) of the αβTCR. Here, the αβTCR mainly binds to two α-helices of the globin fold in the PE α-subunit, which is analogous to the antigen-binding platform of the MHC molecule. Using retrogenic mice expressing this TCR, we show that it supports intrathymic T cell development, maturation, and exit into the periphery as mature CD4/CD8 double negative (DN) T cells with TCR-mediated functional capacity. Accordingly, we show how an αβTCR can recognise an intact foreign protein in an antibody-like manner.

Antibodies and T cells play a central role in adaptive immunity. Antibodies directly bind to intact antigens, such as proteins and carbohydrates, typically with very high affinity, and have been broadly used for numerous immunotherapies. In contrast, αβ T cells, which express heterodimeric αβ T cell antigen receptors (αβTCRs) on their cell surface, interact with fragments of foreign or self-peptides (p) that are presented by molecules encoded by the Major Histocompatibility Complex (MHC). The simultaneous co-recognition of peptide and

[1]Department of Microbiology & Immunology, Peter Doherty Institute for Infection and Immunity, University of Melbourne, Melbourne, VIC, Australia. [2]Infection and Immunity Program and Department of Biochemistry and Molecular Biology, Biomedicine Discovery Institute, Monash University, Clayton, VIC, Australia. [3]European Molecular Biology Laboratory (EMBL) Australia Node in Single Molecule Science, School of Medical Sciences, University of New South Wales, New South Wales, Australia. [4]Melbourne Protein Characterisation Platform, Bio21 Molecular Science and Biotechnology Institute, Melbourne, VIC, Australia. [5]Division of Rheumatology, Inflammation, and Immunity, Brigham and Women's Hospital, Harvard Medical School, Boston, MA, USA. [6]Department of Infectious Diseases and Immunology, Faculty of Veterinary Medicine, Utrecht University, Utrecht, The Netherlands. [7]Stratingh Institute for Chemistry, University of Groningen, Groningen, The Netherlands. [8]Institute of Infection and Immunity, Cardiff University School of Medicine, Heath Park, Cardiff, UK. [9]Present address: Department of Microbiology and Immunology, at the Peter Doherty Institute for Infection and Immunity, University of Melbourne, Melbourne, Victoria, Australia. [10]These authors contributed equally: Catarina F. Almeida, Benjamin S. Gully. [11]These authors jointly supervised this work: Adam P. Uldrich, Jamie Rossjohn, Dale I. Godfrey. ✉e-mail: auldrich@unimelb.edu.au; Jamie.rossjohn@monash.edu; godfrey@unimelb.edu.au

MHC molecules by the αβTCR is known as MHC restriction[1–3], a central paradigm in the field of immunology that has shaped our understanding of T cell development, function and dysfunction.

In addition to αβTCR recognition of pMHC complexes, αβTCRs interact with lipids and metabolite-based antigens presented by MHC-I like molecules, namely CD1 and MR1, respectively[2]. Here, in general, αβTCR ligation conforms to the co-recognition paradigm, although some autoreactive TCRs can directly recognise CD1a[4,5] and CD1c[6] while not contacting the lipid antigens bound within the antigen-binding cleft. Thus, αβTCRs can bind to antigen presenting molecules in a variety of modalities, but nevertheless invoke recognition of MHC or MHC-I-like molecules. How αβTCRs can bind other distinct molecules remains unclear.

In contrast to conventional T cells, γδ T cells exhibit greater diversity in ligands that can activate them. Namely, human and mouse γδ T cells recognise antigen-presenting molecules such as MHC-I, MHC-II, endothelial protein C receptor, CD1 and MR1, or stress-inducible molecules that possess the MHC-I fold, via their γδTCR[7–19]. Other γδ T cells are activated by more structurally distinct ligands, such as butyrophilin (BTN)-mediated sensing of phosphorylated prenyl metabolites, or BTN-like molecules[20–23]; reviewed in refs. 24,25. Moreover, both human and mouse γδTCRs have been reported to recognise other intact antigens, such as phycoerythrin (PE), independently of cellular antigen-presentation[26], thereby further highlighting the versatility of TCR recognition.

In engineered mice deficient in MHC and the CD4 and CD8 receptors, or Lck mutant mice, αβ T cells were identified that expressed αβTCRs that did not interact with MHC, but directly recognised intact antigens[27,28]. Specifically, many of these non-MHC restricted TCRs recognised CD155, an adhesion molecule that is ubiquitously expressed in the thymus. Moreover, the adhesion molecules CD48 and CD102 have been described as ligands for non-MHC-restricted αβTCRs[29]. Two such CD155-reactive TCRs (termed B12A and A11) adopt the same canonical structures of MHC-restricted αβTCRs, but bound to CD155 with high (nanomolar) affinity[30], whereas MHC-restricted αβTCRs generally bind with weaker (micromolar) affinity, reviewed in Ref. 2. Negative-stain electron microscopy and mutational analyses indicated that these αβTCRs bound to the N-terminal domain of CD155, although the atomic basis underpinning direct αβTCR recognition of CD155 remains obscure.

Here, we characterise an αβ T cell clone that directly recognises, through its TCR, a foreign protein, R-phycoerythrin (PE), independently of antigen presenting molecules. The TCR was previously isolated from a Jα18$^{-/-}$ BALB/c mice that expressed MHC and the CD4/CD8 coreceptors. This TCR supported intrathymic T cell development with a bias toward CD4$^-$CD8$^-$ DN T cells. The crystal structure showed that six αβTCR molecules engaged the same epitope of each PE molecule within a hexameric complex of PE heterodimers. Accordingly, this study demonstrates the existence of an αβTCR that can directly bind a foreign protein with a mechanism akin to that of antibodies, a finding that falls outside the classical understanding of how αβTCR recognise ligands.

Results

Exploring reactivity of TCRs isolated with CD1d tetramers

We previously characterised Natural Killer T (NKT) cell clones in Jα18$^{-/-}$ BALB/c mice that lack the most common NKT TCRs, using mouse CD1d-α-glucuronosyl-diacylglycerol (α-GlcADAG) and CD1d-α-galactosylceramide (α-GalCer) tetramers that were conjugated with streptavidin (SAV)-PE and SAV-Brilliant Violet(BV)421, respectively[31]. Among the population that co-bound both tetramers, several non-canonical Vα10 Jα50 TCR rearrangements were identified. Within the CD1d-α-GlcADAG tetramer$^+$ CD1d-α-GalCer tetramer$^-$ population, two distinct TRAV4 (Vα11) TCR rearrangements were identified, namely TRAV4-2$^+$ ("A11B8.2", Vα11 Jα9 Vβ8.2$^+$ TCR) and TRAV4D4$^+$ ("4D4", Vα11 Jα4 Vβ10$^+$ TCR). The former clone was observed with a high frequency among sorted thymic clones from the same sample and reacted with CD1d-α-GlcADAG[31], whereas the 4D4 clone remained uncharacterised.

To investigate if the 4D4 TCR sequence conferred reactivity towards CD1d-α-GlcADAG, we generated TCR-transduced BW58 cell lines (4D4 TCR.BW58 reporter line), alongside four others: the previously published α-GlcADAG reactive NKT TCRs (A11B8.2 and A10B8.2), an α-GalCer-reactive type I NKT TCR ("VB8-STD", Vα14 Jα18 Vβ8$^+$)[32], and sulfatide-reactive ("XV19", Vα1 Jα26 Vβ16$^+$) type II NKT TCR[33]. Next, PE-conjugated CD1d tetramers that were either unloaded (thus containing endogenous antigens incorporated during CD1d expression), or loaded with exogenous α-GlcADAG, α-GalCer or sulfatide, were used to assess antigen reactivity of the transduced cell lines by flow cytometry (Fig. 1A). As expected, the VB8-STD type I NKT TCR and XV19 type II NKT TCR preferentially bound to CD1d carrying α-GalCer and sulfatide, respectively, while the A11B8.2 and A10B8.2 NKT TCRs bound CD1d-α-GlcADAG. Interestingly, the 4D4 TCR$^+$ cell line reacted with all CD1d tetramers, regardless of the antigen loaded into CD1d. To investigate if the 4D4 TCR expressed by this cell line could induce a functional response following CD1d-antigen recognition, plate-bound activation assays with CD1d were undertaken (Fig. 1B). While the A11B8.2, A10B8.2, VB8STD TCR$^+$ cell lines responded to CD1d loaded with their cognate antigens, the 4D4 TCR was unresponsive to CD1d loaded with any antigen (Fig. 1B). This suggested that, despite staining with CD1d tetramers, the 4D4 TCR was not CD1d-reactive.

Identification of a PE-reactive αβ T cell clone

Next, we tested the 4D4 cell line with CD1d tetramers conjugated with a different fluorochrome, namely BV421. Here, biotinylated CD1d loaded with α-GalCer was tetramerised using either SAV-PE or SAV-BV421, and used to stain the 4D4 TCR$^+$ cell line or a CD1d-α-GalCer reactive control NKT cell line expressing the A10B8.2 NKT TCR[31]. Both 4D4 and A10B8.2 TCR$^+$ cell lines stained with PE-labelled CD1d-α-GalCer tetramers (MFIs of 19738 and 13094, respectively, Fig. 1C top) however, while the A10B8.2 NKT TCR$^+$ cell line was also stained by BV421 labelled CD1d-α-GalCer tetramers (MFI 25148, Fig. 1C bottom), the 4D4 TCR$^+$ cell line was not (MFI 387, Fig. 1C bottom). This suggested that the 4D4 TCR was recognising the PE molecule, which is notably a known antigen for B cells[34,35] and γδ T cells[26]. We also identified γδTCRs derived from peripheral blood samples from healthy donors that bound to phycobiliprotein-based fluorescent tags, including clones 1C5H, BC14PE1, BC14PE3 which bound to PE, and also the clone HD1APC, which selectively bound to allophycocyanin (APC) but not PE-conjugated SAV (Supplementary Fig. 1). Therefore, the ability of different streptavidin-fluorochrome conjugates (PE, PE-Cy7, APC, APC-Cy7, BV421, Pacific Blue (PB)) to stain each of the 4D4 and A10B8.2 TCR$^+$ cell lines was assessed. Whilst both the SAV-PE and SAV-PE-Cy7 specifically stained the 4D4 TCR$^+$ cell line (Fig. 1D), the other SAV-conjugates did not, supporting the hypothesis that the 4D4 TCR binds specifically to PE-containing molecules.

Interestingly, when testing PE that was not conjugated to SAV sourced from two different suppliers, 'Prozyme' and 'Thermo Fisher Scientific', (Fig. 1E) we observed that only PE from Prozyme, but not from Thermo Fisher Scientific, stained the 4D4 TCR$^+$ cell line. PE is a hexameric complex molecule formed by six α and six β subunits that are organised symmetrically around a single γ subunit. PE isoforms from different species of algae exhibit variability in the amino acid sequence or position and number of chromophores within each subunit[36]. Consistent with this notion, denaturing polyacrylamide gel electrophoresis (SDS-PAGE) analysis of PE sourced from Prozyme contained two variants of the γ chain subunit with distinct apparent sizes (28 kDa and 31 kDa), while the α and β subunits were similar sizes (~18k Da), and co-migrated (Fig. 1E). PE sourced from Thermo Fisher

https://doi.org/10.1038/s41467-024-51897-3

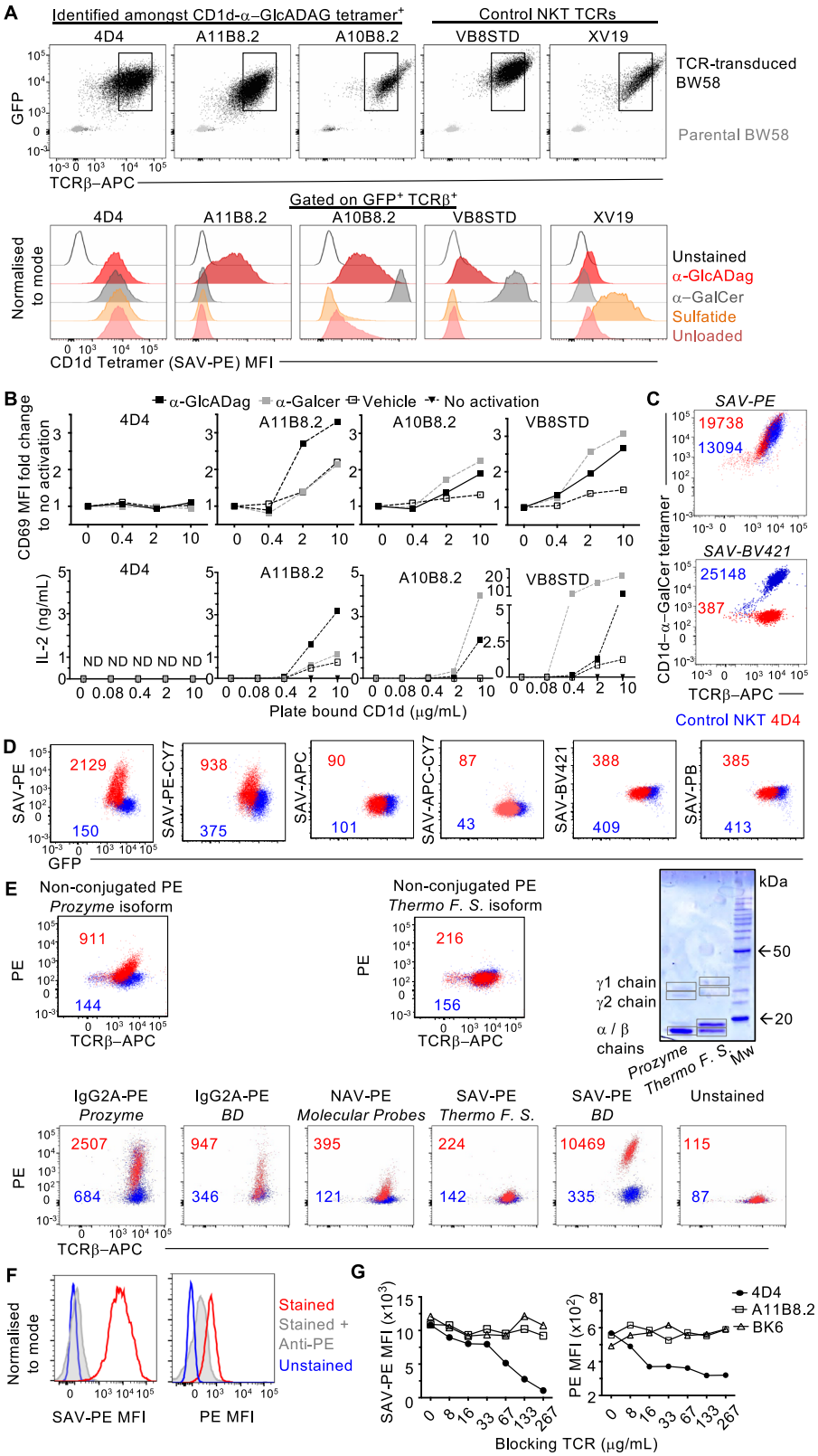

Scientific is derived from *Porphyra tenera*, and also contained two variant γ chains (29 and 32 kDa), but these were distinct to the Prozyme reagent γ chains. Additionally, unlike the PE isoform sourced from Prozyme, both α and β chains (18 and 19 kDa) could be distinguished. These results suggest that the PE isoform sourced from Prozyme (red algae of undisclosed species) is distinct to that sourced from Thermo Fisher Scientific (*Porphyra tenera*). Various forms of PE conjugates were also tested for their ability to stain the 4D4 TCR$^+$ cell line (Fig. 1E). In agreement with the staining by non-conjugated PE sourced from Prozyme, a conjugated form of PE (IgG2a-PE) from the same supplier also stained the 4D4 TCR$^+$ cell line but not the control NKT TCR$^+$ cell line. Additionally, IgG2a or SAV-conjugated PE from an alternative manufacturer (Becton Dickinson, (BD)) also stained the 4D4 TCR$^+$ cell line. Likewise, neutravidin (NAV)-conjugated PE from Molecular Probes

Fig. 1 | PE binds to 4D4 TCR$^+$ cells. A BW58 cells were transduced with the 4D4 TCR sequence which was identified amongst single cell BALB/c Jα18$^{-/-}$ thymocytes sorted as CD1d-α-GlcADAG-tetramer-(SAV-PE)$^+$ CD1d-α-GalCer-tetramer (SAV-BV421)$^-$ (as per Almeida et al, 2019) and assessed for binding to α-GlcADAG-, α-GalCer-, sulfatide-loaded or unloaded CD1d tetramers (SAV-PE conjugated). Flow cytometry plots show TCRβ versus GFP expression on top and mean fluorescence intensity (MFI) of SAV-PE conjugated tetramers on TCRβ$^+$GFP$^+$ gated cells. CD1d-α-GlcADAG-reactive (A11B8.2 and A10B8.2, CD1d-sulfatide-reactive (XV19) and CD1d-α-GalCer-reactive VB8-STD TCR-expressing clones were included as controls. **B** Graded amounts of plate-bound CD1d loaded with α-GlcADAG, α-GalCer or vehicle (Veh) were assessed for their ability to activate the 4D4 clone compared to A11B8.2, A10B8.2 or VB8-STD control lines. Plots show flow cytometric detection of CD69 upregulation (mean of 2 experiments) or IL-2 secretion using a capture bead assay after 16 h. **C** α-GalCer-loaded CD1d was tetramerised using SAV-PE (top plot) or SAV-BV421 (bottom plot) and assessed for staining of the BW58 lines expressing the 4D4 TCR (red) or control A10B8.2 TCR (blue) by flow cytometry. **D** SAV-PE, SAV-PE-CY7, SAV-APC, SAV-APC-CY7, SAV-BV421, and SAV-PB (all from Becton Dickinson) were assessed for their ability to stain the 4D4 (red) or the control V1168 NKT (blue) TCR+ lines. **E** Two distinct isoforms of non-conjugated PE (from Prozyme and from Thermo Fisher Scientific) were assessed for their ability to stain 4D4 (red) or control A10B8.2 (blue) TCR+ cell lines, and analysed in a 10% SDS-PAGE gel (top). The ability of different PE conjugates (from the indicated suppliers) to stain the same cell lines was investigated by flow cytometry (bottom). **F** Anti-PE mAb (50μg/ml) or **G** soluble 4D4 TCR, and the control A11B8.2 NKT TCR or CD1a-restricted BK6 TCR were pre-incubated with SAV-PE or PE alone and assessed for impact on staining by FACS of the 4D4 cell line. Data in Fig. 1A–G are representative of 2 independent experiments, except for the gel in **E**, which was one of two runs (reducing and non-reducing) from one experiment, and the BK6 control in **G** which was used in one experiment. Source data are provided as a Source Data file.

also stained the 4D4 TCR$^+$ cells, albeit to a lesser extent than the Prozyme and BD reagents. Consistent with the lack of staining by non-conjugated PE sourced from Thermo Fisher Scientific, SAV-conjugated PE from the same supplier also failed to stain the 4D4 TCR$^+$ cell line. These results suggested that the 4D4 TCR can only bind PE from certain species, as was previously observed for PE-reactive γδTCRs[26].

Next, we investigated if the interaction between PE and 4D4 TCR on the 4D4 TCR$^+$ cell line could be blocked by competition with an anti-PE mAb or the soluble 4D4 TCR ectodomain. Staining was blocked by pre-treatment with anti-PE mAb (Fig. 1F) and soluble 4D4 TCR, but not with two irrelevant TCRs (the A11B8.2 mouse CD1d-restricted NKT TCR and the BK6 human CD1a-restricted TCR[4]) (Fig. 1G). Collectively, these results indicate that the 4D4 TCR directly interacts with some forms of PE in the absence of antigen-presenting molecules.

4D4 αβTCR$^+$ T cells are activated by immobilised PE

Next, non-conjugated PE, or SAV- and NAV-conjugated PE from different suppliers were tested for their ability to activate the 4D4 TCR$^+$ cell line. The 4D4 TCR$^+$ and VII68 NKT TCR$^+$[33,37] cell lines responded to stimulation with anti-CD3 mAb (Fig. 2A). Consistent with the requirement of CD3/TCR crosslinking, only plate-bound anti-CD3 mAb could induce activation of the BW58 reporter cell lines, as measured by IL-2 production, when compared to anti-CD3 mAb in solution. Consistent with the PE staining assays (Fig. 1D, E), plate-bound non-conjugated PE from Prozyme, SAV-conjugated PE or PE-Cy7 from BD, and NAV-PE from Molecular Probes elicited IL-2 production by the 4D4 TCR$^+$ cell line but not by the VII68 control NKT cell line (Fig. 2A), whilst other SAV-fluorochrome conjugates failed to elicit a response. This shows that ligation of the 4D4 TCR by PE, in the absence of antigen-presenting cells, could activate the 4D4 cell line. When non-conjugated PE or SAV- and NAV-conjugated PE were added in solution, the 4D4 TCR$^+$ cells failed to respond, suggesting that the 4D4 TCR requires cross-linking for activation. Consistent with the lack of staining by SAV-PE sourced from Thermo Fisher Scientific in Fig. 1E, this SAV-PE conjugate failed to induce IL-2 production by the 4D4 TCR$^+$ cells either in solution or when plate bound.

The ability to block PE-induced activation was also explored, using a neutralising anti-PE mAb that was added after the plates were coated with PE, SAV-PE, SAV-FITC or SAV-APC. Additionally, the phycobiliproteins were heated to 90 °C prior to use, in order to denature the fluorochromes[38] (Fig. 2B). Here, PE-induced activation of the 4D4 TCR$^+$ cell line (by either SAV-conjugated or non-conjugated PE) was blocked either by heat-inactivation or by anti-PE mAb addition to the culture, suggesting that the 4D4 TCR recognises a conformational epitope in PE. Together, these findings demonstrate that the 4D4 TCR specifically binds PE isoforms, and cross-linking of 4D4 TCR$^+$ cells results in activation in the absence of APCs or antigen-presenting molecules.

We also investigated whether PE-ligation could modulate the surface-expression of CD69, CD44, CD25 activation markers, and/or CD3/TCR expression levels, using the 4D4 TCR$^+$ cell line (Fig. 2C) as well as the 1C5H TCR$^+$ Jurkat line (Supplementary Fig. 2). Mitogenic control stimulation using plate-bound anti-CD3 is consistent with the fact that Jurkat cell lines are not capable of upregulating CD25. Notably, only when there was a strong CD69 increase (in response to SAV-PE—which bound strongly to 4D4 (Fig. 1D, E), or to control anti-CD3 stimulation), did we observe TCR/CD3 downmodulation, and slight CD44 upregulation, and also CD25 in the 4D4 TCR$^+$ cell line. We detected CD69 upregulation, in response to plate bound SAV-PE and SAV-PECy7 conjugates, in the 4D4 and 1C5H TCR$^+$ lines, but not in the control CD1d-restricted TCR$^+$ lines (VII68 and 9C2[9]), nor in response to other SAV-controls and non-conjugated SAV (Fig. 2C). Notably, NAV-PE stimulation, which binds weakly to 4D4 (Fig. 1E) and elicits IL-2 production (Fig. 2A), did not drive CD69 upregulation in the 4D4 TCR$^+$ cell line, despite doing so in the 1C5H.TCR.Jurkat line (Supplementary Fig. 2A). Neither of these cell lines responded to the non-fused NAV-control. Akin to the 4D4 line (Fig. 2B and 2C), 1C5H also failed to respond to heat-inactivated SAV-PE (Supplementary Fig. 2A).

Antigen-presenting cells can express receptors that can bind PE, such as FcγRI receptors[39–41] or B cell receptors[34,35,42]. To investigate if soluble PE was immobilised and presented by antigen-presenting cells, we co-cultured 4D4 TCR$^+$ cells or 1C5H.TCR.Jurkat lines with K562 or human monocyte derived DCs in the presence of SAV-PE, SAV-BV421, or anti-CD3 and assessed CD69 upregulation and TCR downmodulation. Whereas activation of the 4D4 clone by soluble SAV-PE was not detected in any of the tests, the 1C5H line upregulated CD69 in response to soluble SAV-PE, even in the absence of other antigen-presenting cells (Supplementary Fig. 2B). These results suggest that the 1C5H.TCR.Jurkat line can immobilise and present PE antigens.

Next, we investigated if 4D4 TCR$^+$ cells could be activated by mouse dendritic cells expressing CD1d. Here, 4D4 TCR$^+$ cells, or control type I NKT 2C12 TCR$^+$ cells, were co-cultured with bone marrow-derived dendritic cells (BMDC) from C57BL/6 WT or CD1d$^{-/-}$ mice Supplementary Fig. 3A). IL-2 was detected at high levels in the co-culture supernatant of 2C12 TCR$^+$ cells with BMDC WT in the presence of α-GalCer and, to a lesser extent, α-GlcADAG, and even in the absence of exogenously added-ligand (Supplementary Fig. 3B). Importantly this was prevented by anti-CD1d blocking mAb added at the beginning of culture, or when 2C12 was co-cultured with BMDC CD1d$^{-/-}$, indicating CD1d-dependent activation. In contrast, 4D4 TCR$^+$ cells were not activated in this context, regardless of the lipid antigen and presence or absence of CD1d. While we also found that neither of the TCR$^+$ cell lines responded specifically to PE added to BMDC-co-cultures, in comparison to BMDC-co-cultures with no exogenous ligand added, this is in line with our observations in Supplementary Fig. 2 where PE loaded into cellular cocultures did not stimulate 4D4 TCR$^+$ cells. Using a plate-bound assay, as expected, high levels of IL-2, and upregulation of CD69, were detected when 2C12 TCR$^+$ cells were cultured with plate-immobilised CD1d-α-GalCer and, albeit less so, CD1d-α-GlcADAG and

https://doi.org/10.1038/s41467-024-51897-3

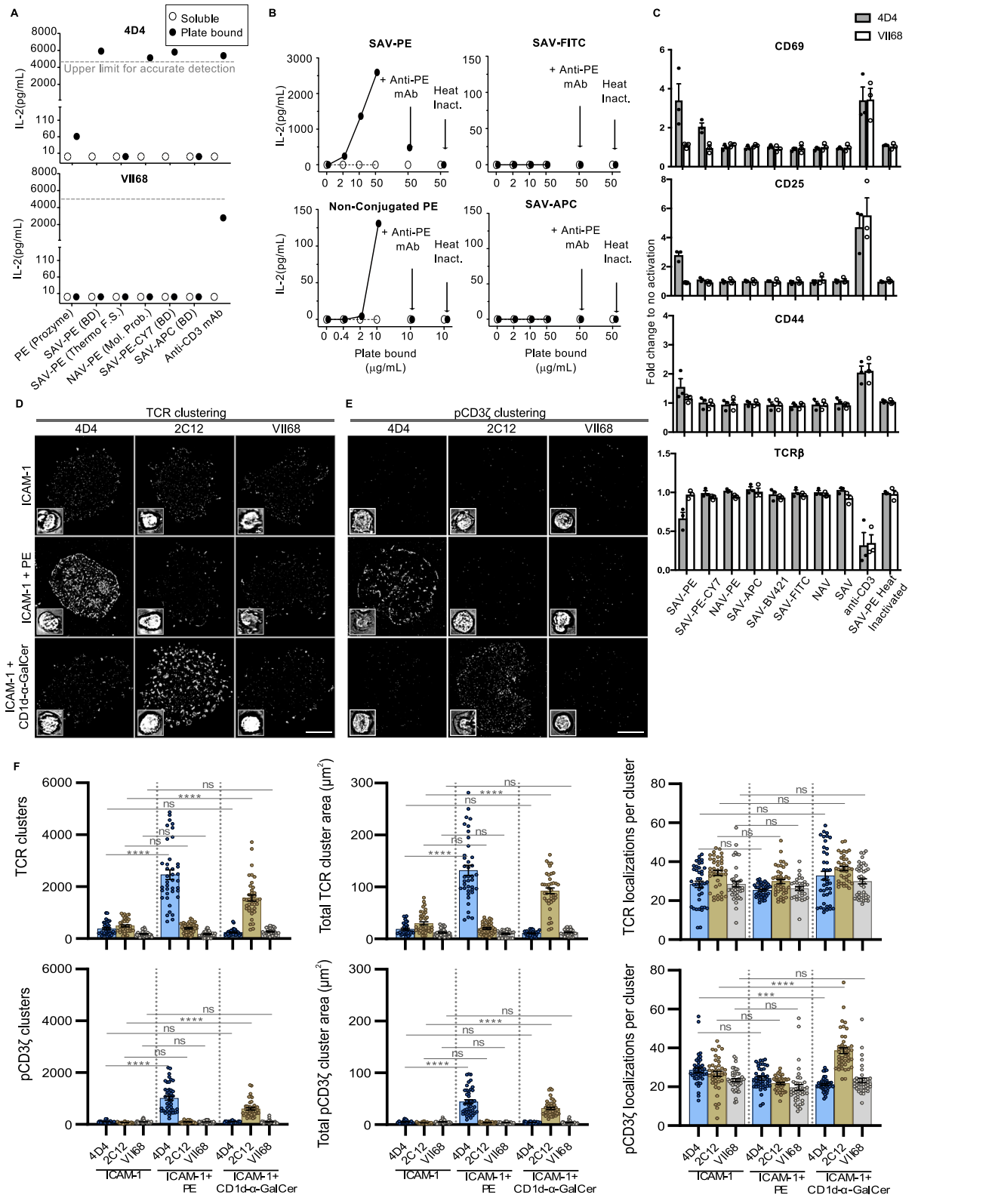

CD1d-endo, which is loaded with a vast array of self-lipids incorporated into CD1d during its synthesis[43] (Supplementary Fig. 3C). This again shows that the type I NKT 2C12 TCR can be activated by a range of CD1d-bound lipids. In contrast, 4D4 was not activated by any of these plate-bound CD1d-lipid antigen complexes but was clearly activated (based on IL-2 and CD69) by plate-immobilised PE. Both TCR-transduced lines responded to plate-bound anti-CD3 (Supplementary Fig. 3C). Thus, these data are all consistent with the concept that the 4D4 TCR is not CD1d-restricted.

Next, we investigated ligand-induced TCR cluster formation using single-molecule imaging of antibodies against CD3ε (Fig. 2D, Supplementary Fig. 4 and Supplementary Table 1) and phosphorylated CD3ζ (pCD3ζ) (Fig. 2E and Supplementary Fig. 4). We exposed BW58 cell lines expressing the 4D4 TCR or the control 2C12 type I NKT TCR[32] to

Fig. 2 | PE activates cells expressing the 4D4 TCR. A Plate bound or soluble versions of non-conjugated PE (from Prozyme) and various forms of SAV-conjugated PE (from different suppliers) at 50 or 100 µg/mL−respectively−were assessed for their ability to activate a BW58 cell line expressing the 4D4 TCR or a control NKT TCR (VII68). Anti-CD3 (10 µg/mL) mAb was included as a positive control for stimulation. After 16 h the supernatants were assayed for the presence of IL-2 by cytometric bead array. **B** Titrating amounts of plate bound SAV-PE, SAV-APC, SAV-FITC and non-conjugated PE were assessed for their ability to elicit IL-2 production by the 4D4 or the control A11B8.2 NKT TCR line. In order to investigate if PE induced activation could be prevented by a neutralising antibody or protein denaturation, the top concentration of each sample was pre-incubated with anti-PE mAb (20µg/ml), or incubated at 90 °C for 2 min. Data in A and B is representative of 2 independent experiments except for the heat-inactivated samples and the SAV-FITC samples in **B** which were one experiment. **C** After 16 h of stimulation with plate bound molecules as indicated, 4D4 (grey bar) or VII68 (white bar) cells were stained for CD44, CD69 CD25 or TCRβ surface expression. Mean Fluorescence Intensity fold variation relative to no activation, error bars represent ± SEM for each marker across 3 independent experiments, each represented by the individual dots. Single-molecule imaging of TCRβ (**D**), or pCD3ζ (**E**), clustering in BW58 thymoma cells transduced with the 4D4, 2C12 or VII68 TCRs following stimulation on a supported lipid bilayer decorated with either ICAM-1 only, ICAM-1 and SAV-PE or ICAM-1 and CD1d-α-GalCer. Inset bright-field images show thymoma cells used for single-molecule imaging. Scale bar: 5 µm. **F** Single-molecule data were analysed using DBSCAN across three experiments with a total number of cells (shown as dots) TCRβ /pCD3ζ for ICAM-1; 4D4 (40/42), 2C12 (40/42), VII68 (40/42), for PE; 4D4 (40/44), 2C12 (42/42), VII68 (42/40) and for CD1d-α-GalCer; 4D4 (40/45), 2C12 (39/44), VII68 (40/40). Data were expressed as mean ± SEM. One-way ANOVA was used for comparing stimulation against an ICAM-1 control. ns = not significant. $^{*}P \le 0.05$; $^{**}P \le 0.01$; $^{***}P \le 0.001$; $^{****}P \le 0.0001$ (exact P values shown in Supplementary Table 1). Source data provided as a Source Data File.

supported lipid bilayers containing either ICAM-1 only as an negative control, or ICAM-1 with either SAV-PE or CD1d-α-GalCer, alongside a positive control of anti-CD3 and anti-CD28 mAb-induced activation. The number and size of TCR clusters increased significantly for both the 4D4 and 2C12 TCRs in response to SAV-PE and CD1d-α-GalCer, respectively, although the TCR localisations per cluster remained unchanged throughout (Fig. 2F and Supplementary Fig. 4). In addition to forming ligand-induced dense TCR clusters in response to their cognate ligands, both the 2C12 and 4D4 TCRs potently phosphorylated CD3ζ (Fig. 2F and Supplementary Fig. 4). The number and size of pCD3ζ clusters increased significantly for 2C12 and 4D4 TCRs in response to CD1d-α-GalCer and SAV-PE, respectively. The CD1d-endo specific VII68 type II NKT TCR, which is not α-GalCer-reactive, remained unresponsive to either ligand. Thus, proximal signalling of the 4D4 TCR is specifically induced upon recognition of PE and leads to potent CD3ζ phosphorylation.

4D4 αβTCR directly binds PE

We next explored whether the 4D4 TCR interacts with PE in biochemical cell-free assays. Given that PE is a large (>240 kDa) hexameric complex of heterodimers that coordinate a central γ−subunit $[(\alpha\beta)_6\gamma]$[36], we hypothesised that each PE has more than one site that could be recognised by the 4D4 TCR.

To initially estimate the TCR:PE stoichiometry, we employed sedimentation velocity analytical ultracentrifugation (SV-AUC). Here the 4D4 TCR existed as heterodimeric species with a sedimentation coefficient $S_{20,w} = 3.7$, and a frictional ration $f/f_o = 1.3$ with a derived estimated molecular weight (MW) of 51 kDa, in close agreement with the theoretical value (50.25 kDa) (Fig. 3A and Supplementary Fig. 5). As expected, PE was larger ($S_{20,w} = 11.4$, $f/f_o = 1.3$), with a corresponding estimated MW of 255 kDa (Fig. 3A and Supplementary Fig. 5), similar to the theoretical MW (~265 kDa). Complexation at a 10-fold molar excess of TCR to PE resulted in a complex peak at $S_{20,w} = 13.7$, $f/f_o = 1.6$ with a MW estimation of 471 kDa corresponding to approximately four 4D4 TCRs (estimated MW = 51 kDa) bound to PE (estimated MW = 268 kDa) (Fig. 3A and Supplementary Fig. 5). Indeed, free monomeric TCR was present in the complex sample, suggestive of over-saturation at a 10:1 TCR:PE molar ratio. Additional SV-AUC experiments with a 3:1, 4:1, 5:1 and 6:1 molar excess of the 4D4 TCR revealed an increasing complex mass $S_{20,w} = 12.5$, 12.7, 13.0 & 13.1, respectively, with MW estimations suggesting approximately four 4D4 TCRs bound to the PE molecule (471 kDa) (Fig. 3B). To further refine the estimated stoichiometry, samples containing soluble 4D4 TCR and PE mixed at different molar ratios (1:1-7:1) were analysed by electrophoretic mobility shift assay. Figure 3C shows that the band corresponding to soluble 4D4 TCR alone can be distinguished from that of PE alone, reflecting the differences in charge and size between the two molecules. The TCR−PE complex appeared to progressively increase in size from the 1:1 up to the 6:1 molar ratio, with no additional increase at the 7:1 ratio. A clear band corresponding to unconjugated TCR was also seen at this ratio, suggesting a maximum of six TCRs per PE molecule.

We employed isothermal titration calorimetry (ITC) to further estimate the interaction affinity values and determine the stoichiometry of the 4D4 TCR - PE interaction. These data suggested that the interaction between 4D4 TCR and PE was characterised by a detectable change in enthalpy (ΔH of −7731 cal/mol) and entropy (ΔS of −0.145 cal/mol/deg), as averaged from two separate experiments (Fig. 3D). This change in enthalpy was similar to what has been described for most αβTCR-pMHC interactions[44,45]. The estimated stoichiometry of binding (n) of TCR per PE molecule was 4.79 ($n = 3.89$ in a first experiment under limiting TCR conditions, and $n = 5.7$ when the TCR was saturating), with an affinity (K_D) value of 2.3 µM. Collectively, this data suggested that up to six molecules of soluble 4D4 TCR could bind to each PE heterodimer within the hexamer.

Finally, we measured the affinity of the 4D4 TCR for PE using surface plasmon resonance (SPR). Three distinct strategies were employed: firstly, non-conjugated PE (Prozyme) was immobilised on the sensor directly by amine coupling. Secondly, the same non-conjugated PE isoform was indirectly captured via an immobilised anti-PE polyclonal antibody (pAb). Thirdly, SAV-conjugated PE (BD), or control SAV-APC (BD) was immobilised via amine coupling. Soluble 4D4 TCR, or control VII68 (type II NKT) αβTCR were injected over the chip at graded concentrations. Binding of soluble 4D4 TCR to PE was clearly detected, but not to the APC or anti-PE pAb alone control ligands, relative to a control (empty) flow cell (Supplementary Fig. 6). The control VII68 TCR did not bind to any of the ligands tested, supporting the specificity of the 4D4 TCR interaction with PE. The saturation plots derived at equilibrium for each condition were consistent with a one site binding model and facilitated the determination of equilibrium constant (K_D) values (Supplementary Fig. 6). The interaction between the 4D4 TCR and directly coupled PE had a similar affinity to the indirectly coupled PE ($K_D = 4.9$ µM and 3.3 µM, respectively), as did the interaction between SAV-PE and 4D4 TCR ($K_D = 5.3$ µM). These K_D values are similar to those described for PE-reactive γδTCRs ($K_D = 2.7$ µM by SPR)[26]. In a separate SPR experiment we tested the specificity of the 4D4 TCR against mouse MHC and MHC-like molecules (Fig. 3E). Here, the 4D4 TCR specifically bound to PE and showed little or no binding to CD1d-α-GalCer, I-A^b-CLIP, H2-D^b-NP_{366} and MR1-5-OP-RU (Fig. 3E). The control 2C12 NKT TCR bound specifically to CD1d-α-GalCer and showed no specific binding to other molecules tested. We next conducted SPR with an expanded CD1d panel. Here the 4D4 TCR did not significantly bind to CD1d endogenously loaded with a multitude of distinct self-lipids during production (CD1d-endo). Such a very weak response is within the noise of SPR experiments. Moreover, we observed no binding to CD1d-α-GalCer or CD1d-α-GlcADAG (Supplementary Fig. 7). These SPR-based results are consistent with no 4D4 TCR mediated reactivity or activation to CD1d-endo across our other experiments. The control NKT TCRs 2C12 and

https://doi.org/10.1038/s41467-024-51897-3

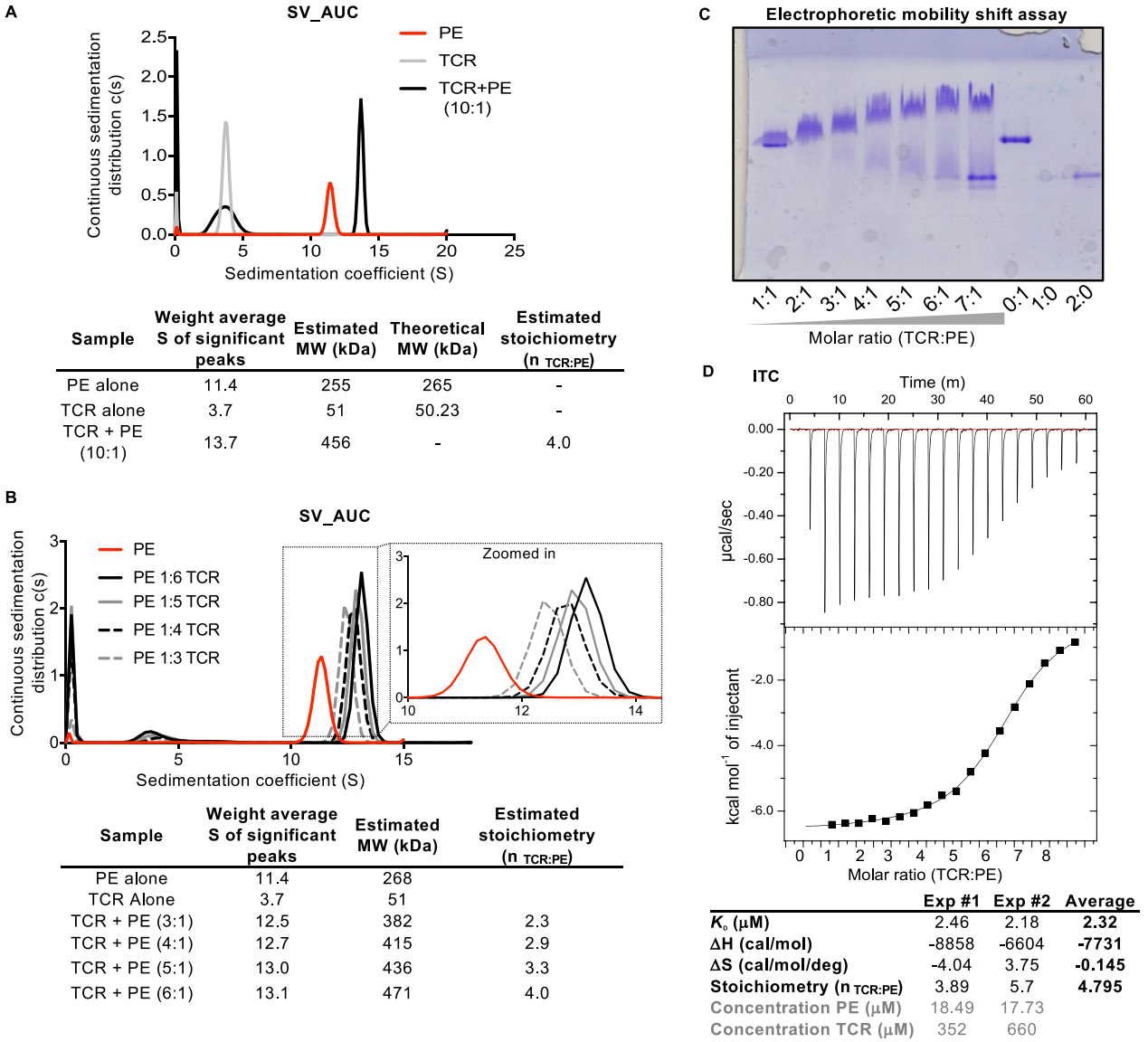

Sample	Weight average S of significant peaks	Estimated MW (kDa)	Theoretical MW (kDa)	Estimated stoichiometry (n TCR:PE)
PE alone	11.4	255	265	-
TCR alone	3.7	51	50.23	-
TCR + PE (10:1)	13.7	456	-	4.0

Sample	Weight average S of significant peaks	Estimated MW (kDa)	Estimated stoichiometry (n TCR:PE)
PE alone	11.4	268	
TCR Alone	3.7	51	
TCR + PE (3:1)	12.5	382	2.3
TCR + PE (4:1)	12.7	415	2.9
TCR + PE (5:1)	13.0	436	3.3
TCR + PE (6:1)	13.1	471	4.0

	Exp #1	Exp #2	Average
K_D (µM)	2.46	2.18	**2.32**
ΔH (cal/mol)	-8858	-6604	**-7731**
ΔS (cal/mol/deg)	-4.04	3.75	**-0.145**
Stoichiometry (n TCR:PE)	3.89	5.7	**4.795**
Concentration PE (µM)	18.49	17.73	
Concentration TCR (µM)	352	660	

A11B8.2[31] confirmed the quality and loading of the CD1d samples, showing CD1d-α-GalCer specificity and the preferentially CD1d-α-GlcADAG reactivity, respectively. Accordingly, this 4D4 TCR does not exhibit notable cross-reactivity to a panel of MHC and MHC-like molecules including CD1d loaded with a range of lipid-based antigens. Collectively, these experiments indicated that the soluble 4D4 TCR directly interacts with PE with an affinity that is comparable to that of functional αβTCR-peptide MHC interactions[2].

Structural basis of the 4D4 αβTCR-PE interaction

To further understand the molecular basis of the 4D4 TCR's recognition of PE, we first solved the structure of PE from Prozyme (purified from source), to 2.0 Å via X-ray crystallography (Supplementary Table 2 and Supplementary Fig. 8). These structural data revealed the classical globin-like fold of the heterodimeric PE α and β subunits which each comprised of a nine-helix bundle (X, Y, A, B, E, F, F′, G and H)[46–48] (Supplementary Fig. 8A, B). Here, PE heterodimers oligomerised

https://doi.org/10.1038/s41467-024-51897-3

Fig. 3 | Biophysical analysis of the 4D4 interaction with PE. A Size distribution plot derived from sedimentation velocity analysis in an analytical ultracentrifuge (SV-AUC). Data is shown for soluble 4D4 TCR alone, PE alone or a mixture of both at a 10:1 (TCR:PE) molar ratio. Sedimentation coefficient (S) was determined and used to calculate the molecular weight (MW) of each component in solution. The estimated MW of the complex was compared to the MW of PE alone and used to estimate the molar binding ratio of TCR:PE (n), as shown in the table below. **B** On a separate SV-AUC experiment 4D4 TCR was incubated at different ratios with a fixed amount of PE (3:1-6:1 TCR:PE molar ratio), results are presented as in **A**. In the zoomed region of the graph, numbers on top of peaks represent S for each sample. **A**, **B** are representative of 2 independent SV-AUC experiments. **C** Electrophoresis mobility shift assay: 4D4 TCR was incubated at different ratios (1:1–7:1) with a fixed amount of PE and complex formation investigated in a 7.5% native PAGE gel. On separate wells PE or 4D4 were ran alone. Data is representative of 2 independent assays. **D** Representative Isothermal titration calorimetry trace (upper) and binding isotherm (lower) following serial injections of soluble 4D4 TCR (17.7 µM) into a PE solution (Prozyme; 660 µM). The addition of buffer alone (PBS pH 8) to PE and of PE to buffer alone were subtracted from the values presented to exclude buffer induced heat fluctuations. Data is representative of two independent experiments. The dissociation constant (K_D), stoichiometry of binding (n), enthalpy (ΔH) and entropy (ΔS) for the binding reaction were estimated for each experiment and averaged, as shown in the table below. **E** Surface plasmon resonance of the 4D4 TCR and 2C12 type I NKT TCR binding to immobilised PE, mouse (m)CD1d-α-GalCer, I-A^b-CLIP, H2-D^b-NP_{366} and mMR1-5-OP-RU. Data are shown for two independent SPR experiments, each colour coded as orange and blue, with the equilibrium binding curves plotting the mean derived from two SPR runs per experiment, used to estimate the dissociation constant (K_D). N.D. = not determined. Source data are provided as a Source Data file.

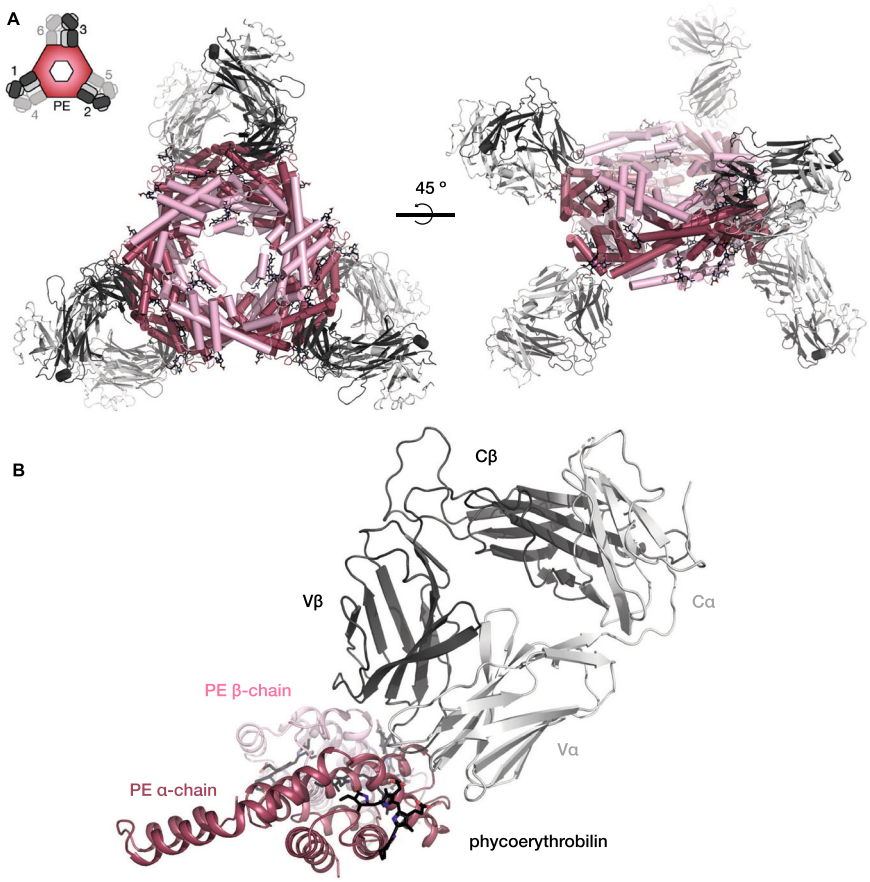

Fig. 4 | Overall architecture of the 4D4 TCR-PE complex and recognition mode. A Cartoon representation of the symmetry-expanded 4D4 TCR–PE complex, showing the 4D4 TCR (grey) interface recognising a symmetry-related epitope upon the hetero-hexameric PE assembly (red). **B** The asymmetric unit of the 4D4 TCR–PE complex (4D4 TCR and PE α- and β-chains shown, light grey, dark grey, dark red, and pink, respectively).

to form a hetero-hexameric arrangement comprised of two face-to-face $\alpha_3\beta_3$ hetero-trimers related by a two-fold symmetry axis with the γ subunit remaining unresolved (Supplementary Fig. 8C).

Informed by the unbound PE structure, we next determined the co-complex structure of the 4D4 TCR bound to PE at 3.0 Å using X-ray crystallography (Supplementary Table 2 and Fig. 4). The asymmetric unit showed the 4D4 TCR bound the PE α-chain and hence there were six 4D4 TCRs bound to the hetero-hexameric PE when considering the symmetry-related chains (Fig. 4A). The antigen-binding variable domains of the 4D4 TCR docked orthogonally over the A-B and E helices of the PE α-chain with the TCR constant domains extending away from the interface (Fig. 4B). The total buried surface area (BSA) at the interface was 1465 $Å^2$ of which the TCR α- and β- chains contributed 44% and 55% BSA to the interface, respectively (Fig. 5A, B). The 4D4 TCR-PE interface included both germline and non-germline residues with each of the complementarity determining regions (CDR) involved in the interface but most prominently involved the CDR1α, CDR3α and CDR3β which contributed 18%, 24% and 52% of the BSA, respectively (Fig. 5B).

These CDR mediated interface contacts included R30α of the CDR1α which formed a salt bridge with D57 of the B-helix of the PE α-chain whereby the arginine sidechain was stabilised by the

https://doi.org/10.1038/s41467-024-51897-3

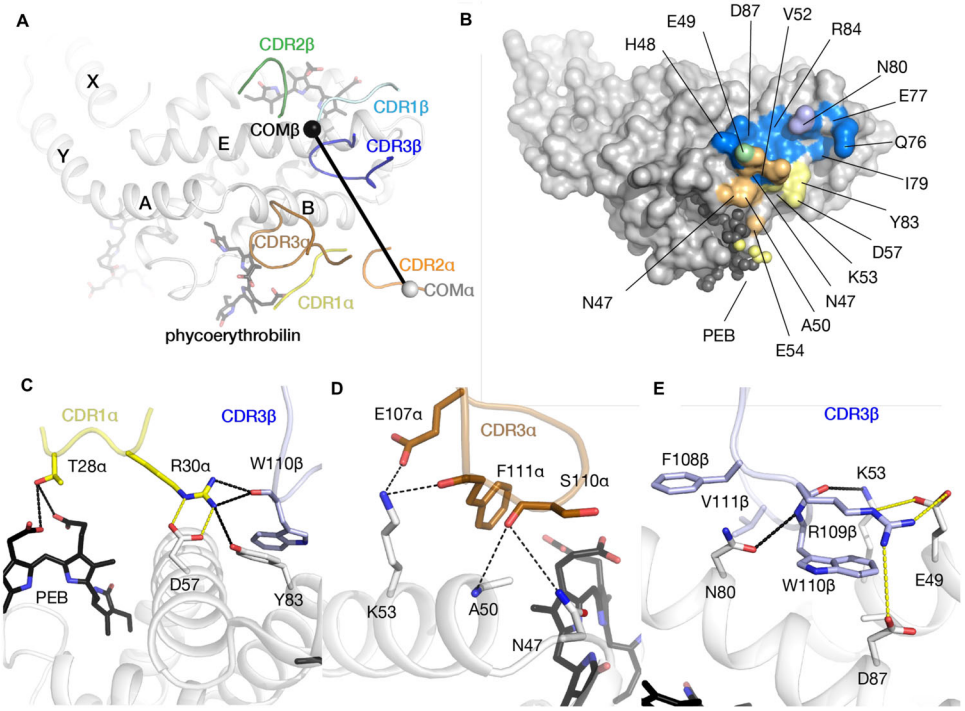

Fig. 5 | Molecular interactions at the 4D4 TCR-PE interface. A Complementarity determining region (CDR)-mediated contacts from the 4D4 TCR to PE and the molecular contacts therein (**B**). The CDR loops are coloured as follows: CDR1α yellow, CDR2α orange, CDR3α wheat, CDR1β light blue, CDR2β light green, CDR3β dark blue on the PE α-chain show as grey cartoon, with the Vα and Vβ centres of mass (COM) shown as grey and black spheres, respectively. The molecular surface is coloured according to the respective CDR-mediated contacts. The 4D4 TCR α-chain interactions from the CDR1α and CDR3α are shown in (**C**, **D**). The 4D4 TCR β-chain interactions from the CDR3β are shown in (**E**). Hydrogen and Van der Waals interactions are shown in black with salt bridge contacts shown as yellow dashed lines.

neighbouring Y83 of the PE E-helix and W110 of the CDR3β (Fig. 5C). The CDR3α was germline encoded and made contacts via E107α and F111α to the K53 sidechain of PE, and via S110α, to N47 and A50 of the B-helix of the PE α-chain (Fig. 5D). The 4D4 TCR-PE interface also included notable β-chain contacts that were heavily dominated by the CDR3β loop (Fig. 5E) which comprised half of the BSA owing to a cluster of hydrophobic residues (F108β, W110β and V111β), of which F108β and V111β were non-germline-encoded, and W110β was encoded by TRBD2. Here W110β extended the CDR3β loop and protruded into a cleft comprised by the A, B and E helices of the PE α-chain and formed an array of van der Waals (VDW) and electrostatic contacts (Supplementary Table 3, Fig. 5E). These CDR3β contacts were stabilised by R109β which made a salt bridge interaction with E49 with additional contact to D87 of PE so as to cap W110β within the helical bundle (Fig. 5E).

The germline encoded T28α of the CDR1α loop contacted the carboxyethyl group of the second pyrrole ring of one of two phycoerythrobilin (PEB) chromophores within the PE α-chain (Supplementary Table 3, Fig. 5C), with this PEB covalently linked to C139. Comparison of the two structures highlighted a remarkable conservation of the PE α-chain pre- and post- 4D4 TCR engagement, notwithstanding a ~1 Å movement of the PEB carboxyethyl group upon TCR binding. Thus, the structure of the 4D4 TCR in complex with PE revealed the direct antigen recognition capacity of an αβ T cell to an intact protein antigen, through a mechanism that is highly dependent on contacts via the hypervariable CDR3 loops of the TCR. To provide insight into species-specific reactivity to PE from the 4D4 TCR, we conducted multiple sequence alignments of ~150 bacterial PE α-chains and visualised this in the context of the structure. Mapping the sequence variation and conservation within the PE epitope recognised by the 4D4 TCR was relatively conserved across different bacterial species (Supplementary Fig. 9 and Supplementary Table 4).

The PE structural epitope recognised by 4D4 TCR harboured an MHC-like helical arrangement. Indeed, alignment of the A, B & E helices of the PE α-chain globin-like fold to MHC and MHC-like molecules showed architectural homology, although the helices ran in opposing directions (Fig. 6A–I). The closest mimics to the structural epitope were other members of the globin-like family including haemoglobin and neuroglobin (root mean square deviation (RMSD) ~ 4 Å) (Fig. 6J–L). More distant epitope homology to MHC and MHC-like molecules was also noted (RMSD ~ 8 Å) although the basis for this homology remains unknown.

PE-reactive αβTCRs support T cell development in vivo

To investigate whether the PE-reactive 4D4 αβTCR can support T cell development in the thymus, we generated retrogenic mice reconstituted with bone marrow transduced with 4D4 TCRα and β-chain that were separated by a self-cleaving 2 A linker[49]. Retroviral-based 4D4 TCR was co-expressed along with reporter GFP amongst TCRβ$^+$ cells. T cell accumulation in the thymus, spleen, lungs, liver and lymph nodes of the C57BL/6 wild type (WT CD45.1) recipients could be detected as early as 10 weeks after bone marrow transfer from *Rag1*$^{-/-}$ CD45.2 retrogenic donors (Fig. 7A). Interestingly, the majority of TCRβ$^+$ GFP$^+$ cells in the thymus were either CD4$^+$ and CD8$^+$ (double positive, DP), or CD4$^-$ and CD8$^-$ (double negative, DN), unlike TCRβ$^+$ GFP$^-$ cells from both retrogenic mice or WT controls, which were mainly CD4$^+$ or CD8$^+$ (Fig. 7B and Supplementary Fig. 10A), as expected from cells that undergo positive selection through interaction with MHC-II and MHC-I molecules, respectively. TCRβ$^+$ GFP$^+$ cells in the periphery, including the lung, were similarly DN in contrast to their TCRβ$^+$ GFP$^-$ counterparts. These results suggest that the thymic selection pathway for the PE-reactive 4D4 TCR does not rely on interactions with MHC molecules. Furthermore, TCRβ^{hi} GFP$^+$ cells derived from retrogenic mice bound to SAV-PE, suggesting that these cells expressed the 4D4 TCR

https://doi.org/10.1038/s41467-024-51897-3

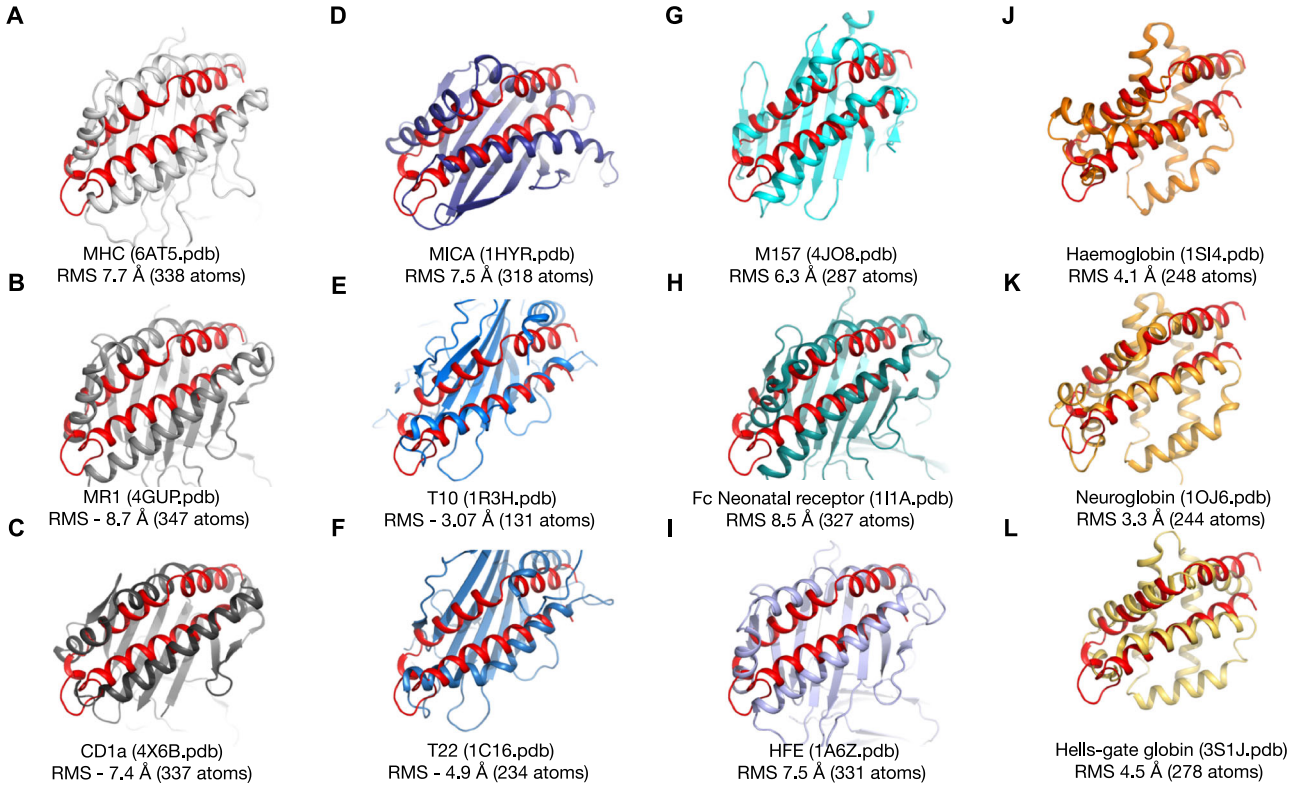

Fig. 6 | Structural homology of the PE paratope recognised by the 4D4 TCR. Cartoon representation and alignment of the PE α-chain paratope (in red) recognised by the 4D4 TCR to; **A** MHC-I[81], **B** MR1[82], **C** CD1a[4], **D** MICA[83], **E** T10[84], **F** T22[85], **G** M157[86], **H** Fc neonatal receptor[87], **I** HFE[88], **J** Haemoglobin[89], **K** Neuroglobin[90], and **L** Hell's gate globin[91].

and had progressed through thymic maturation and were exported into the periphery (Fig. 7C and Supplementary Fig. 10B). To confirm that the 4D4 TCR sequence was indeed expressed in the periphery and corresponded to the GFP reporter signal, we individually sorted viable TCRβ$^+$ cells according to their GFP expression from a retrogenic mouse spleen and determined paired TCR sequences using nested TCR amplification[50] (Fig. 7D). Whilst TCRβ$^+$ GFP$^-$ cells expressed diverse TCRs, TCRβ$^+$ GFP$^+$ expressed the 4D4 TCR (Fig. 7D). We also investigated if 4D4 TCR$^+$ retrogenic cells could respond to PE stimulation by culturing splenocytes from 4D4 TCR$^+$ retrogenic mice or WT mice with plate bound SAV-PE or control SAV-APC, SAV-BV421 or anti-CD3 mAb (Supplementary Fig. 11). 4D4 TCR$^+$ retrogenic cells upregulated the activation markers CD69 and CD25 after 18 h and proliferated after 3 days of culture with immobilised SAV-PE or anti-CD3 mAb, but not to SAV-BV421 or SAV-APC. By contrast, TCRβ$^+$GFP$^-$ cells from the retrogenic mice or from WT mice only responded to anti-CD3 mAb stimulation (Supplementary Fig. 11). Collectively, these experiments demonstrate that PE-binding 4D4 TCR can support intrathymic T cell development, maturation and emigration of DN T cells to peripheral organs, which are functionally active and capable of binding to and responding to immobilised PE in vitro.

Discussion

Our findings provide the molecular basis for direct, antibody-like αβTCR recognition of an intact protein, PE, in the absence of antigen-presenting molecules. Using a broad range of cellular and biophysical assays we validated the specificity of this interaction and determined the crystal structure of this TCR-PE complex. While direct recognition of intact antigens such as PE is a known property of both B cells[34,35] and γδ T cells[26], this is not considered to be a characteristic of αβ T cells, where the paradigm is that they detect antigens presented by antigen-presenting molecules[2].

Presently, a few examples of direct antigen recognition by αβ T cells have been described, where αβTCR recognition of a number of adhesion molecules has been observed[27–29]. However, such T cell clones, unlike 4D4, were derived from mouse models whereby normal events associated to thymic selection were bypassed, involving "QuadKO" all MHC-deficient (*β2m*$^{-/-}$*H-2Ab*$^{-/-}$) and coreceptor-deficient (*CD4*$^{-/-}$*CD8*$^{-/-}$), or Lck deficient mice. It remains unclear whether these cells develop in normal circumstances and persist in a wider and biologically relevant immune context. Interestingly, a highly engineered TCR, derived from molecular evolution experiments targeting the CDR loops, was shown to bind to the side of an MHC-I molecule without contacting the bound peptide, but this TCR recognition mode failed to propagate a T cell activation signal[51]. Nevertheless, naturally occurring human αβTCRs can interact with CD1a[4,5,52,53] and CD1c[6] molecules without contacting the bound lipid antigen, reviewed in Ref. 54.

The reactivity of the 4D4 TCR was largely conferred via the hypervariable CDR3α and CDR3β loops. This could explain why these cells have not previously been detected in naïve mice, due to a reliance on random recombination events and an antigen-specific population that is unlikely to be expanded in mice. While we attempted to find more αβ T cell clones exhibiting such reactivity, we failed to do so, indicating that either this reactivity is very rare, and/or hard to detect. Nonetheless, the ability for αβTCRs to be endowed with direct antigen-binding capacity by their CDR3 regions raises the prospect that this may occur for a range of molecular targets. In line with this hypothesis, the CDR3α loop can confer TCR specificity to three other MHC-independent antigens: CD155, CD48, and CD102[28,55]. The 4D4 TCR–PE structure highlighted the importance of key hydrophobic interactions within the apex of the CDR3β that comprised ~50% of the total interface. Indeed, αβ T cell selection is skewed towards self-reactivity upon the inclusion of hydrophobic residues within the CDR3β[56]. Thus, hydrophobic CDR3 loops may enable unconventional antigen

https://doi.org/10.1038/s41467-024-51897-3

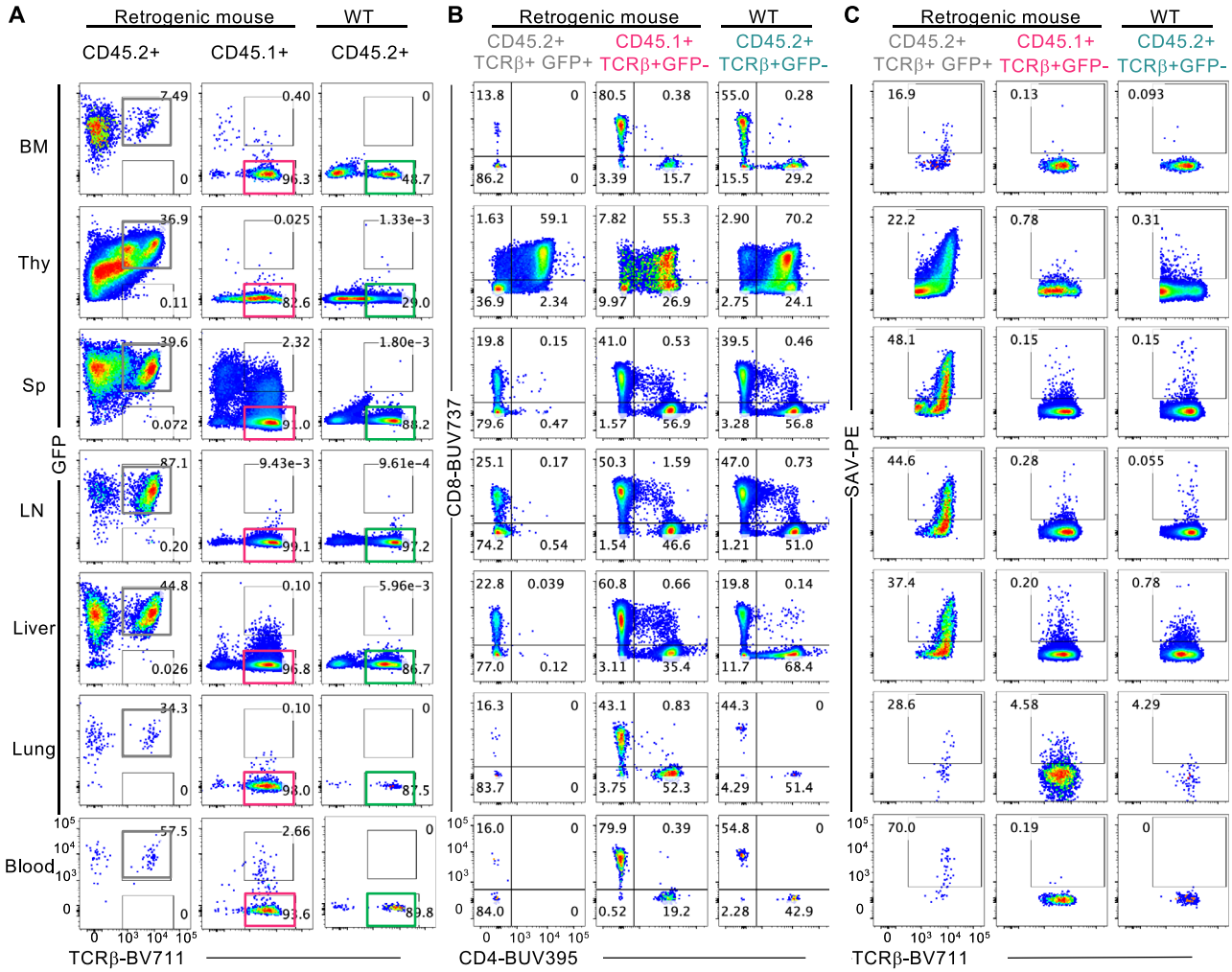

D

	Clone	TRAV	CDR3α	TRAJ	TRBV	CDR3β	TRBJ	TRBDJ
GFP Neg	1	TRAV9D-4	CVLTSSNTNKVVF	TRAJ34	TRBV16	CASSADQNTLYF	TRBJ2-4	TRBD1
GFP Neg	2	TRAV7-1	CAGLWYNQGKLIF	TRAJ23	TRBV16	CASSLENQGSGNTLYF	TRBJ1-3	TRBD1
GFP Neg	3	TRAV7-4	ND	TRAJ17	TRBV14	ND	TRBJ1-1	TRBD1
GFP Neg	4	TRAV6-1	ND	TRAJ6	TRBV29	ND	TRBJ1-2	TRBD1
GFP Neg	5	TRAV5-4	CAASPNTGYQNFYF	TRAJ49	TRBV16	ND	TRBJ2-4	TRBD1
GFP Neg	6	TRAV6-4	ND	TRAJ33	TRBV13-3	CASSDRGGGSQNTLYF	TRBJ2-4	TRBD1
GFP Neg	7	TRAV9N-3	CAVSIAGNTGKLIF	TRAJ37	TRBV15	ND	TRBJ1-1	TRBD1
GFP Neg	8	TRAV9D-4	CVLSYTGYQNFYF	TRAJ49	TRBV16	CASSADVLEQYF	TRBJ2-7	TRBD1
GFP pos	1	TRAV4D-4	CAAEAGSFNKLTF	TRAJ4	TRBV4	CASSFRWVGEQYF	TRBJ2-7	TRBD2
GFP pos	2	TRAV4D-4	CAAEAGSFNKLTF	TRAJ4	TRBV4	CASSFRWVGEQYF	TRBJ2-7	TRBD2
GFP pos	3	TRAV4D-4	CAAEAGSFNKLTF	TRAJ4	TRBV4	CASSFRWVGEQYF	TRBJ2-7	TRBD2
GFP pos	4	TRAV4D-4	CAAEAGSFNKLTF	TRAJ4	TRBV4	CASSFRWVGEQYF	TRBJ2-7	TRBD2
GFP pos	5	TRAV4D-4	CAAEAGSFNKLTF	TRAJ4	TRBV4	CASSFRWVGEQYF	TRBJ2-7	TRBD2
GFP pos	6	TRAV4D-4	CAAEAGSFNKLTF	TRAJ4	TRBV4	CASSFRWVGEQYF	TRBJ2-7	TRBD2
GFP pos	7	TRAV4D-4	CAAEAGSFNKLTF	TRAJ4	TRBV4	CASSFRWVGEQYF	TRBJ2-7	TRBD2
	4D4	**TRAV4D-4**	**CAAEAGSFNKLTF**	**TRAJ4**	**TRBV4**	**CASSFRWVGEQYF**	**TRBJ2-7**	**TRBD2**

recognition mechanisms, interestingly many of the previously identified PE-reactive γδ T cells had receptors encoding such CDR3 loops[57].

The 4D4 TCR-PE structure also illustrated some structural homology to the antigen-binding cleft of MHC molecules and of the more distantly members of the globin family, although the significance of such mimicry remains unclear. Of interest, circulating red blood cells (RBC) have been shown to play a role in modulating immune-responses, although only limited studies have explored the involved mechanisms, reviewed in Ref. 58.

Our data with 4D4 TCR retrogenic mice demonstrated that the 4D4 TCR can support intrathymic T cell development, and exit into the periphery, without expressing CD4 or CD8. Intriguingly, this suggests that PE-reactive αβ T cells might not undergo the same thymic selection process as conventional $CD8^+$ or $CD4^+$ T cells. Indeed, the fact that

Fig. 7 | 4D4 TCR$^+$ T cells develop in vivo in a retrogenic mouse model. A Flow cytometry analysis of bone marrow (BM), thymus (Thy), spleen (Sp), lymph node (LN), liver, lung, and blood of 4D4 retrogenic mice (Rg) or wild type (WT) C57BL/6. Representative plots of GFP and TCRβ expression on 7AAD$^-$ CD19$^-$ CD11b$^-$ cells amongst CD45.2$^+$ (from donor transduced BM) or CD45.1$^+$ (recipient) in Rg mice or CD45.2$^+$ from WT mice. **B** CD4 and CD8 co-receptor expression and **C** SAV-PE binding among CD45.2$^+$ TCRβ$^+$ GFP$^+$ Rg cells in comparison to CD45.1$^+$ TCRβ$^+$ GFP$^-$ cells from the same Rg mice, or CD45.2$^+$ TCRβ$^+$ GFP$^-$ cells from WT mice. Data in (**B**) are from one Rg mouse, representative of $n = 12$ Rg mice (acquired over 5 independent experiments for thymus and spleen, or 3 experiments for blood), $n = 10$ Rg mice for liver and BM (4 experiments), $n = 7$ Rg mice for lung and LN (3 experiments); and from one WT mouse representative of n = 7 WT mice (4 experiments) for spleen and thymus, $n = 6$ WT mice for lung, LN and BM (3 experiments), $n = 4$ WT mice for liver (3 experiments). Data in **(C)** are from one Rg and from one WT mice representative of 2 experiments with $n = 2$ or n = 3 Rg and WT organs, with the exception of the liver which is from 1 experiment with $n = 3$ Rg or $n = 3$ WT mice. Graphs showing assay variation for **(B)** and **(C)** are in Supplementary Fig. 10A and 10B. **D** Paired TCR analysis of single cells sorted as TCRβ$^+$ GFP$^+$ or TCRβ$^+$ GFP$^-$ from the spleen of a retrogenic mouse. Nomenclature as per the IMGT database. Source data are provided as a Source Data file.

these lack CD4 and CD8 highlights their resemblance to the T cells that develop in the QuadKO mice[27,28], suggesting that these cells may arise naturally within the thymus through a non-conventional development pathway (MHC and/or co-receptor independent). Notably, MHC-like molecules such as CD1d and MR1 are involved in thymic selection events that give rise to DN mature αβ T cells amongst the NKT and MAIT cell families, respectively, reviewed in Ref. 59. Although the 4D4 clone was isolated with a CD1d tetramer conjugated to PE and loaded with the glycolipid α-GlcADAG, the reactivity of this TCR was to the fluorochrome −PE, not CD1d−lipid. Thus, CD1d tetramer only stained when it was conjugated to PE, not to other fluorochromes, and PE itself is capable of binding and stimulating 4D4 TCR, whereas CD1d is not. Whilst we did not find any evidence suggesting MHC or CD1d-dependence, we cannot exclude that the 4D4 TCR might still bind to another, as yet unidentified, ligand such as MHC or an MHC-like ligand, possibly via dependence on a particular peptide or lipid-based Ag. Regardless of the selection mechanism, the 4D4 TCR$^+$ T cells responded strongly to immobilised PE in vitro, suggesting that they were functionally mature, although future studies should establish the functionality of these PE-reactive T cells in vivo.

Our findings also raise the question of whether T cells would naturally encounter PE as an antigen. While the significance of immune cells that are capable of detecting PE is unclear, this and related phycobiliproteins, such as phycocyanin, are abundant in edible seaweeds[60], also used as food dyes in candy, dairy products, cake decoration, soft drinks, alcoholic beverages, and can further be found in cosmetics, textiles and pharmaceutical products[61]. Thus, T cells with reactivity to PE and PE-like molecular structures may potentially play a role in immune hypersensitivities. Our results suggest PE molecules need to be immobilised to be able to crosslink the TCRs expressed by 4D4 cells and elicit their activation. In a physiological setting, this mechanism could likely be accomplished by cells expressing receptors that can interact stably with PE, such as FcγRI receptors[39–41], B cell receptors[34,35,42], or even γδ TCRs[26].

The findings here provide an example that shows the potential for αβ T cells to encompass broader antigen recognition than previously thought. In summary, we identified the direct recognition of PE by a peripheral αβ T cell clone and characterised this interaction biochemically and structurally, revealing direct αβTCR recognition of an intact, non-MHC-like protein antigen.

Methods

All research complies with the relevant ethical regulations, including the Australian Office of the Gene Technology Regulator for work with GMOs, and those for mouse experimentation or human sample handling as described below:

Mice

Animal experimentation and sacrifice by carbon dioxide inhalation were conducted following the Australian National Health and Medical Research Council Code of Practice for the Care and Use of Animals for Scientific Purposes guidelines for housing and care of laboratory animals and under approval from the Monash University Animal Ethics Committee (MARP/2016/118 and 2023-40644) or the University of Melbourne (UoM) Animal Ethics Committee (#1513734). C57BL/6 WT and C57BL/6 CD1d$^{-/-}$ were bred and maintained at the Department of Microbiology and Immunology Animal house UoM in specific pathogen-free (SPF) conditions. For the retrogenic mouse experiments all mice were maintained in SPF conditions in the Monash Animal Research Platform (MARP), including C57BL/6 *Rag1*$^{-/-}$ mice, sourced from the Walter and Eliza Hall Institute (WEHI), C57BL/6 Ly5.1 sourced from the Australian Research Council (ARC), or additional C57BL/6 WT bred within MARP. All mice used were 7–10 weeks old, and age and gender-matched per experiment.

Human samples

De-identified human buffy coats from healthy blood donors were obtained, with written informed consent, from the Australian Red Cross Blood Service after approval from the University of Melbourne Human Ethics Committee (#1035100), or from the Brigham and Women's Hospital Specimen Bank, Boston. Peripheral blood mononuclear cells were isolated by density gradient using Ficoll-paque Plus (GE Healthcare #17-1440-02) and cryopreserved in liquid nitrogen for subsequent use.

Identification of human γδ TCR sequences 1c5H, HD1APC, BC14PE3, BC14PE1

Human PBMCs were stained with TCRγδ-PE-Cy7, (clone 11F2, BD Biosciences #655410 1:50) and magnetically enriched in an LS column (Miltenyi, #130042401) with anti-PE beads (Miltenyi, #130048801), following manufacturer's instructions. Enriched cells were expanded in vitro with plate−bound anti-CD3 (clone OKT3 10 µg/ml, Biolegend, #317325), soluble anti-CD28 (CD28.2, 2 µg/ml, Biolegend, #302934), phytohemagglutinin (1 µg/ml, Thermo Fisher Scientific, # 00-4977-93), human IL-2 (200 U/ml, Peprotech, #200-02-100UG), human IL-7 (50 ng/ml, eBioscience, #34-8079-82), and human IL-15 (25 ng/ml, Peprotech, #200-15-11UG). After 48 h, cells were removed from anti-CD3, anti-CD28 and phytohemagglutinin stimulation and allowed to expand for 2 weeks in human IL-2, IL-7 and IL-15 before cryopreservation for subsequent analysis. Cells were cultured in complete culture media consisting of a 1:1 (v/v) mix of RPMI-1640 and AIM-V (#11875093, #12055091) supplemented with 10% (v/v) heat inactivated Foetal Bovine Serum (FBS, #10100147), 2% (v/v) human AB serum (Sigma, #H4522-20ML), penicillin-streptomycin (100 U/ml, #15140122), Glutamax (2 mM, #35050061), sodium pyruvate (#1 mM, #11360070), nonessential amino acids (0.1 mM, #11140050), HEPES buffer (15 mM, pH 7.2-7.5, #15630080), all from Thermo Fisher Scientific, and 2-mercaptoethanol (50 µM, Sigma #M6250-100ML), at 37 °C, 5% CO_2. Cells were restained with surface antibody cocktails (described in flow cytometry section) and CD1b or CD1c tetramers (from NIH, SAV-PE conjugated), individually sorted and TCR Vγ and Vδ transcripts identified by multiplexed PCR as described below.

Identification of 4D4 TCR sequence

The 4D4 TCR sequence was originally identified using nested PCR for paired TCR sequence analysis of single cell-sorted BALB/c Jα18$^{-/-}$ thymocytes that were CD1d-α-GlcADAG tetramer positive (conjugated using SAV-PE) and CD1d-α-GalCer tetramer negative (SAV-BV421),

following CD1d-α-GlcADAG tetramer-associated magnetic bead enrichment, essentially from the assays shown in Ref. 31.

Nested multiplex PCR for TCR transcripts

cDNA from individually sorted cells was generated by the addition of 2 µl per well of buffer containing SuperScript VILO (Invitrogen, #11756050) and 0.1% Triton X-100 (Sigma, #T8787) following manufacturer's instructions. cDNA was amplified by two rounds of multiplex nested PCR with a panel of TCR *Vα*-specific and *Vβ* primers, as described[50], or *V*γ-specific and *V*δ primers (Supplementary Table 5) and GoTaq Master Mix (Promega, #M7133). PCR products were separated on a 1.5% agarose gel, purified and sequenced (Australian Genome Research Facility, University of Melbourne), and analysed using the IMGT® database.

Generation of stable TCR-transduced cell lines

TCR constructs containing full-length TCRα and TCRβ or TCRγ and TCRδ chains separated by a 2A-cleavable linker were produced (Genscript) and cloned into pMSCV-IRES-GFP II (pMIG II) vector containing a *cis*-acting hydrolase element P2A-linked gene system (Addgene plasmid #52107). TCR inserts were sequence verified using plasmid specific primers (Supplementary Table 5). HEK293T cells (maintained in house > 10 years) were co-transfected using FuGENE-6 transfection reagent (Promega, #E5911) with pMIGII expression vector containing TCR, pMIGII expression vector containing the mouse or human CD3 subunits[62], packaging vectors pEQ-PAM3-E and pVSV-G[49]. Supernatant containing retroviral particles was collected every 12 h, filtered using a 0.45 µm filter (Sartorius) and used to transduce mouse BW5147.TCR $\alpha^-\beta^-$ thymoma cells (termed BW58; maintained in house > 10 years), for mouse αβTCRs or SKW3 and Jurkat76 cells for human and γδTCRs. The pMIG II, expression and packaging vectors were provided by Dr. Dario Vignali (St. Jude's Research Hospital, USA), and the mouse CD3 expression vector was provided by Prof. Stephen Turner (Monash University, Australia). Cell lines were cultured in complete culture media (DMEM for BW58 or RPMI-1640 for Jurkats) supplemented with 10% FBS (v/v), 15 mM HEPES, 1 mM sodium pyruvate, 0.1 mM non-essential amino acids, 50 µM β-mercaptoethanol, 100 U/mL penicillin, 100 µg/mL streptomycin and 2 mM Glutamax (all from Thermo Fisher Scientific, catalogue numbers described in human culture media section), at 37 °C, 5% CO_2. $CD3^+GFP^+$ cells were sorted by flow cytometry to generate stable lines.

Generation of retrogenic mice

Retrogenic mice expressing the 4D4 TCR were generated by reconstitution of irradiated C57BL/6 CD45.1 mice with retrovirally-transduced bone marrow cells (CD45.2) using established techniques[49,63]. Firstly, GP + E86 (a retrovirus packaging cell line; maintained in house >10 years) were transduced every 12 h with 0.45 µM filtered supernatant derived from HEK293T cells containing retroviral particles encoding the 4D4 TCR, as described above for generation of stable TCR-transduced cell lines, seven times in the presence of 6 µg/ml polybrene (Sigma) in complete DMEM. The GP + E86 4D4 TCR retroviral producer cell line was then grown to confluency in complete DMEM, GFP expression on >80% of cells was confirmed by flow cytometry and stocks were frozen down for subsequent use. Next, C57BL/6 *Rag1*$^{-/-}$ mice were injected i.p. with 150 mg/kg of 5-fluorouracil (Sigma); bone marrow was harvested 72 h later and bone marrow cells were cultured for 48 h in complete DMEM with 20% FBS, 20 ng/ml murine IL−3, 50 ng/ml human IL−6 and 50 ng/ml murine stem cell factor (SCF) (Biosource International, Camarillo, CA). Bone marrow cells were then transduced by co-culture with irradiated (1200 rads) GP + E86 4D4 TCR retroviral producer cells for 48 h in complete DMEM with 20% FBS plus 6 µg/ml polybrene, 20 ng/ml murine IL−3, 50 ng/ml human IL−6 and 50 ng/ml murine SCF. Non-adherent transduced bone marrow cells were removed from the GP + E86 producer cells, washed and resuspended in PBS containing 20 units/ml Heparin (Sigma), and injected i.v. at ~4×10^6 cells/mouse into irradiated (two doses of 550 rads 3 h apart) C57BL/6 WT recipients (~1 donor/1 recipient). Bone marrow reconstitution was verified 10 weeks after transplant by analysis of blood leucocytes. To validate 4D4 TCR sequence expression, retrogenic mouse spleen were individually sorted based on GFP and TCRβ co-expression and single cell paired TCRα and TCRβ sequences were determined using nested TCR sequencing (as described above).

CD1d production

Mouse CD1d produced in mammalian HEK-293S N-acetylglucosaminyltransferase-I$^-$ (*GnTI*$^-$) (maintained in house > 10 years) cells by co-transfection with pHLsec vectors encoding truncated mouse CD1d ectodomain with a C-terminal biotinylation motif and His6-tag (amino acid sequence at the C-terminus: GSGLNDIFEAQKIEWHEHHHHHH) and β2-microglobulin, using polyethylenimine essentially as described[64]. CD1d was purified from culture supernatant by immobilised metal-affinity chromatography and size-exclusion chromatography, followed by enzymatic biotinylation using biotin ligase (produced in-house), and further purification by size-exclusion chromatography, followed by storage at −80 °C. Production and purification of human CD1b and CD1c followed a similar strategy.

Glycolipids

α-GalCer (C24:1 'PBS-44') was provided by Prof. Paul Savage (Brigham Young University, USA). α-GlcADAG (C19:0/C16:0), was produced and supplied by Dr. Benjamin Cao (from Prof. Spencer Williams laboratory, Bio21 institute, The University of Melbourne, Australia) as described[65]. α-GalCer (C26:0) was purchased from Alexis Biochemicals and Sulfatide (C24:1) was purchased from Avanti Polar Lipids. Glycolipids were prepared in tyloxapol (tyl)-based detergent (0.05% v/v tyl in tris buffered saline solution (TBS) pH 8, and, where indicated, loaded at 6:1 or 12:1 molar ratio overnight at RT, into CD1d. For CD1d tetramerization, SAV-PE or SAV-BV421 (BD Biosciences) was sequentially added to a 1:4 (SAV:CD1d-biotin) molar ratio, following lipid-loading.

Flow cytometry

Livers were perfused using cold PBS, and liver lymphocytes were isolated following a 33% v/v isotonic Percoll (Cytiva, # 17-0891-01) gradient. Bloods were harvested into 0.5 M EDTA, centrifuged at 10,000 g for 10 min, and further purified using a gradient enrichment (Histopaque-1083; Sigma, #10831). Lymphocytes from the thymus, spleen, liver, peripheral lymph nodes, bone marrow bloods and lungs were then incubated with red blood cell lysis buffer (Sigma, #R7757-100ML). Cell suspensions were first incubated for 10 min on ice with Fc-receptor block (anti-mouse CD16/CD32, clone 2.4G2; produced in house, or anti-human (Miltenyi, #130-059-901), both 1:50), prior to antibody staining. Fluorochrome-conjugated mouse-specific antibodies were from BD Biosciences unless otherwise stated: anti-mouse TCRβ-AF700 (eBiosciences, #25-5961-82; 1:100)/BV421 (#562839; 1:200)/APC (#553174; 1:100)/BV711 (#563135; 1:400)/BV786 (#742484; 1:200)—all clone H57-597, CD69-APC/BUV797 (clone H1.2F3, #560016/ #612793; both 1:100), CD25 BV605 (clone PC61, #563061; 1:200), CD44-AF700 (clone IM7, #560567), CD4-BUV395 (clone RM4-5, #740208; 1:400), CD8-BUV797 (clone 53-6.7; 1:800), CD11c-APC-Cy7/ BV421 (clone HL3, #561241, #562782; 1:400), CD1d-BV711 (clone 1B1, #740711; 1:200), CD11b-APC-Cy7 (clone M1/70, #557657; 1:200), B220-BUV496 (clone RA3-6B2, #612950, 1:400), CD19 APC-Cy7 (clone 6D5, #11530; 1:100), CD3 BUV395 (clone 17A2, #740268; 1:100), CD45.2 APC (clone 104, #109814; 1:100), CD45.1 BV786 (clone A20, #740889; 1:200). Anti-human CD25-BV605 (clone 2A3, #562661; 1:100), CD3-BV421 / BUV395 (clone UCHT1, #562426 / #563546; 1:200/ 1:100), CD44-AF700 (clone IM7, eBioscience #56-0441-82), CD69-BUV737 (clone FN50, #612817; 1:100), CD4-BV421 (clone RPA-T4, Biolegend #300532; 1:400), TCRγδ-PE-Cy7/ FITC (clone 11F2, #655410/ #347903;

1:50/ 1:25), TCR δ1-FITC (clone TS-1, Invitrogen #TCR2055; 1:50), 7-amino-actinomycin D (7AAD, Sigma #A9400; 1:300) or Near Infra-Red (NIR 780-Thermo Fisher Scientific, #L34992; 1:400) viability dyes were included in all flow cytometry-staining panels for dead cell exclusion. Streptavidin (SAV)-PE (#554061), SAV-APC (#554067), APC-Cy7 (#554063), SAV-PE-Cy7 (#557598) were purchased from BD Biosciences. SAV-BV421 (#405225) from Biolegend. SAV-PB (#S11222), SAV-PE (#S868, Supplementary Fig. 1D), SAV-APC (#S866, Supplementary Fig. 1C, D) or Neutravidin (NAV)-PE (#A-2660) were purchased from Molecular Probes. All SAV-NAV conjugates were used at 1 μg/mL for BW58 cell line staining for flow cytometry, or 5 μg/mL for retrogenic/WT mice primary cell staining (Fig. 7) flow cytometry analysis of cell lines, or 5 μg/mL for mouse primary cell staining (WT and retrogenic, Non-conjugated R-PE was purchased from Prozyme (undisclosed biological source, #PB31-10MG) or Thermo Fisher Scientific (*Porphyra Tenera,* #46185), both also used at 1 μg/mL for cell staining for flow cytometry. Anti-PE was purchased from Biolegend (#408102) for blocking experiments (Figs. 1F and 2B). Cells were analysed on a BD LSRFortessa II™ or alternatively, single cells were sorted on a BD FACSAria III™ directly into 96-well plates. Samples were analysed using FlowJo version 8 or 10 software. Gating strategies applied shown in Supplementary Fig. 12.

Plate-bound activation assays

Lipid-loaded mouse CD1d, non-conjugated PE (Prozyme, #PB-31-10MG), SAV- IgG- or NAV- conjugated PE, SAV-PE-Cy7, SAV-BV421, SAV-APC or SAV-FITC (all BD Biosciences; catalogue numbers described above), were diluted to working concentrations (as indicated in the figures) in PBS, with 50 μl added to 96-well flat-bottom plates for 3 hours at 37 °C. Where indicated purified NAV (Thermo Fisher Scientific #31000) and purified SAV (MABtech) were included as controls. For thermal denaturation assays, SAV-PE, SAV-APC, SAV-FITC were incubated at 90 °C for 2 min prior to being added to the plate. Anti-mouse or anti-human CD3 (clones 145-2C11, BD, #553057, or OKT3, eBiosciences #14-0037-82) were included as positive controls. All unbound molecules were washed twice from plates with PBS. TCR-transduced cell lines (3.0×10^5 per well) were co-cultured with plate bound complex for 16–18 h in complete DMEM. Cells were labelled with CD69, CD44, and CD25 mAbs to assess upregulation of these activation markers, as well as anti-TCRβ (or anti-CD3 for Jurkat lines expressing human TCRs in Supplementary Fig. 2) and 7AAD.

Cell division of 4D4 TCR retrogenic splenocytes was traced with Cell Trace Violet (CTV, Thermo Fisher Scientific, #34557) at day 3. Culture supernatants of mouse BW58 lines were collected for IL-2 cytokine analysis using cytometric bead array flex set for mice (BD Biosciences, #558297), according to the manufacturer's instructions.

BMDC generation

C57BL/6 WT or $CD1d^{-/-}$ BMDCs were prepared in the presence of GM-CSF (20 ng/ml, Peprotech, #315-03), and IL-4 (5 ng/ml, Peprotech, #214-14), as previously established[66]. Essentially, the culture medium was replaced at day 3 with fresh media with GMCSF and IL-4. Cells were cultured for another 4 days. On day 7 over 95% of cells were $CD11c^+$.

Preparation of Supported Lipid Bilayer (SLB)

Glass coverslips of 0.17 mm thickness were thoroughly cleaned in the order of 1 M KOH, rinsed with Milli-Q water, and finally placed in 100 % (v/v) ethanol accordingly. Glass coverslips were dried inside a fume hood to evaporate off ethanol, followed by plasma cleaning. Coverslips were the adhered to eight-well silicon chambers (Ibidi, #80841). A 1 mg/mL liposome solution was subjected to vesicle extrusion in order to prepare the SLB as previously described elsewhere[67]. The lipid composition of liposomes include 96.5 % DOPC (1,2-dioleoyl-sn-glycero-3-phosphocholine), 2 % DGS-NTA(Ni) (1,2-dioleoyl-sn- glycero-3-[(N-(5-amino-1-carboxypentyl)iminodiacetic acid)succinyl] (nickel salt)), 1% Biotinyl-Cap-PE (1,2-dioleoyl-sn-glycero-3-phosphoethanolamine-N-(cap biotinyl) (sodium salt)), and 0.5% PEG5000-PE (1,2-distearoyl-sn-glycero-3-phosphoethanolamine-N-[methoxy(poly-ethylene glycol) −5000] (ammonium salt). All lipids are available from Avanti Polar Lipids (DOPC, #850375 C, DGS- NTA(Niquel), #790404 C, Biotinyl-Cap-PE, #870273 C, PEG5000-PE, #880220 C). Extruded liposomes were added to eight-well chambers at a ratio of 1:5 with Milli-Q water and 10 mM of $CaCl_2$. Liposomes were incubated for 30 min at RT and then gently rinsed with PBS repeatedly. The disruption to SLB was minimised by retaining ~200 μL of PBS in each well during washing steps. Fluorescence recovery after photobleaching (FRAP) was carried out using fluorescent streptavidin (Invitrogen, #S11223) to examine the lateral mobility of freshly prepared SLB[67]. Excess Ca^{2+} ions on SLB were removed by the addition of 0.5 mM EDTA, followed by gentle rinsing with Milli-Q water. The functionalised NTA groups in DGS-NTA(Ni) lipids were recharged by adding 1 mM $NiCl_2$ solution to SLB for 15 min. Excess Ni^{2+} ions were removed by repeated washing with PBS.

Stimulating BW58 thymoma cells on SLB

To further functionalise the SLB, 500 ng/mL of SAV-PE (BD Pharmingen, #554061) was directly coupled with the biotin groups on SLB. Prior to coupling 500 ng/mL of biotinylated mouse CD1d-α-GalCer or 500 ng/mL of biotinylated anti-mouse CD3 (Invitrogen, #13-0031-82, clone 145-2C11) and anti-mouse CD28 mAbs (Invitrogen, #13-0281-82, clone 37.51), 100 μg/mL of streptavidin with no fluorochrome (Invitrogen, #434301) was directly coupled to SLB. For unstimulated BW58 cell controls, 200 ng/mL of His-tagged mouse ICAM-1 (Sino Biological, #50440-MO8H) was directly coupled with NTA groups on the SLB. After decorating with different ligands, SLB was repeatedly rinsed with PBS to remove excess unbound proteins. Before adding BW58 thymoma cells expressing different TCRs, SLB was incubated with warm RPMI culture medium (37 °C) for 30 min. Thymoma cells were then allowed to activate on SLB for 5 min at 37 °C, followed by immediate cell fixation with 4% (v/v) paraformaldehyde in PBS for 15 min. Excess fixatives were removed by rinsing with PBS.

Immunostaining of BW58 cells

Prior to immunostaining, BW58 cells were permeabilised with 0.1% (v/v) Triton X-100 (Sigma-Aldrich, #T8787) for 15 min and then rinsed with PBS. Cells were then blocked with 5% (w/v) bovine serum albumin in PBS solution to reduce non-specific binding. TCRs expressed on BW58 cells were stained using primary antibodies reactive against the TCRβ subunit and conjugated to Alexa Fluor 647 fluorophore (clone H57-597, BioLegend, #109218). In parallel, under same conditions, a separate set of thymoma cells were stimulated on SLB and stained with primary antibodies reactive against pCD3ζ-Alexa Fluor 647 (BD Biosciences, #558402) to detect phosphorylation on the CD3 complex. Antibody staining was performed for 1 h at RT. Afterwards, samples were repeatedly rinsed with PBS to remove excess unbound antibodies. Post fixation step was carried out using 4% (v/v) paraformaldehyde in PBS for 15 min. Finally, prior to imaging, 0.1 μm TetraSpeck microspheres (Invitrogen, #T7279) were embedded onto the SLB.

Single-molecule imaging with direct stochastic optical reconstruction microscopy (dSTORM)

Imaging buffer consisting of TN buffer (50 mM Tris-HCl pH 8.0, 10 mM NaCl), oxygen scavenger system GLOX [0.5 mg/mL glucose oxidase (Sigma-Aldrich, #G2133); 40 mg/mL catalase (Sigma- Aldrich, #C-100); and 10% (w/v) glucose], and 10 mM 2-aminoethanethiol (MEA; Sigma-Aldrich, #M6500) was used for single-molecule imaging with *d*STORM. Image sequences for *d*STORM were acquired on a total internal reflection fluorescence (TIRF) microscope (commercial setup, Nanoimager by ONI) equipped with a 100x (1.4NA) oil immersion objective, XYZ closed-loop piezo stage, and lasers 405 nm (150 mW), 473 nm (1 W), 561 nm (1 W) and 640 nm (1 W). Prior to imaging,

Nanoimager was temperature stabilised at 30 °C. Time series of 10,000 frames were acquired per sample, under 30% of 640 nm and 10% of 405 nm laser power with an exposure time of 30 ms, at near-TIRF angle of 54°. Prior to acquiring time series, a photobleaching step was carried out for 10–20 s using 90% 640 nm laser power to reduce fluorescence signal emanating from phycoerythrin as a consequence of spectral bleed through to far-red channel. Fluorescence detection was done by sCMOS camera (ORCA Flash 4, Hamamatsu). Image processing, including fiducial marker-based drift correction and generation of x-y particle coordinates for each localisation was carried out by ONI proprietary software (version 1.16).

Cluster Analysis of single-molecule images

For the detection and quantification of cluster parameters in single-molecule images, a previously published algorithm in MATLAB was used[67]. The density-based spatial clustering of applications with noise (DBSCAN) analysis implemented in MATLAB was used to identify and quantify individual clusters. Here, we pre-determine the minimum number of neighbours (minimum points = 3) and the radius which they occupy ($r = 20$ nm). From this, we calculated the total number of detectable receptor clusters, their total area of occupancy and localisations within each cluster. Statistical analysis was performed using one-way ANOVA. Statistical significance reported by P-values indicated as $^{*}P \le 0.05$, $^{**}P \le 0.01$, $^{***}P \le 0.001$, and $^{****}P \le 0.0001$. Error bars represent the SEM across $n \ge 40$ BW58 cells and >3 independent experiments. All statistical analysis was performed using GraphPad Prism software (version 7.04).

Expression and purification of soluble 4D4 TCR protein and phycoerythrin purification. The cDNA encoding the mouse 4D4 ectodomain was synthesised as individual TCRα and TCRβ and cloned in pET30 (Novagen), expressed, refolded, and purified from *Escherichia coli* inclusion bodies. Inclusion bodies were resuspended in 8 M Urea, 20 mM Tris-HCl (pH 8.0), 0.5 mM sodium-ethylenediaminetetraacetic acid (EDTA), and 1 mM dithiothreitol. The TCR was refolded by rapid dilution into 5 M urea, 100 mM Tris-HCl (pH 8.5), 2 mM Na-EDTA, 400 mM L-arginine-HCl, 0.5 mM oxidised glutathione, 5 mM reduced glutathione[68]. The refolding solution was then dialysed into 20 mM Tris–HCl pH 8.5. Refolding occurred overnight with gentle stirring at 4 °C. Samples were dialysed for 4 h into 100 mM Urea, 10 mM Tris–HCl pH 8.0 followed by two dialysis steps into 10 mM Tris–HCl at pH 8.0 (4 h and overnight consecutively). Refolded TCRs were purified by diethylaminoethanol (DEAE) sepharose anion exchange, followed by Superdex-75 16/60 gel-filtration (GE Healthcare) and anion exchange Mono Q 10/100 GL (GE Healthcare). The molecular weight of soluble refolded TCRs was validated by liquid chromatography (LC) electrospray ionisation time of flight (ESI-TOF) mass spectrometry (MS) (Agilent, Bio 21 institute). Phycoerythrin (Prozyme, #PB-31-10MG) was further purified to homogeneity via Superdex-200 16/60 size exclusion chromatography (GE Healthcare) and buffer exchanged into TBS (10 mM Tris-HCl pH 8.0, 150 mM NaCl) prior to experimentation.

Electrophoretic mobility shift assay

Electrophoretic mobility shift assay was performed as previously described[69]. Briefly, for 4D4 TCR-PE complex analysis, 4D4 TCR was incubated at different molar ratios (1:1–7:1) with a fixed amount of PE (2 µg, Prozyme, #PB-31-10MG) and complex formation investigated in native PAGE gel. In one experiment the gel was composed of 5% Acrylamide stacking gel (pH 8.8) over a 7.5% resolving gel (pH 6.8). In a separate experiment a 10% resolving gel was used instead. Samples were run in 1 M Tris-HCl pH 6.8. All gels were stained with coomassie blue.

Surface plasmon resonance

Initial SPR included SAV-PE, SAV-APC, PE alone which were immobilised on a GLC sensor chip (Bio-Rad) by amine coupling, or alternatively, PE was captured with an immobilised anti-PE pAb (Novus Biologicals, #NB120-7011). Graded concentrations of soluble 4D4 TCR or VII68 TCR were simultaneously passed over test and control surfaces at 30 µl/min using 10 mM HEPES pH 7.4, 150 mM NaCl and 0.005% (v/v) Tween-20 buffer. Data was analysed using ProteOn Manager software version 2.1 (Bio-Rad) and dissociation rate (K_d; $M^{-1}\,s^{-1}$) and half-life ($t_{1/2}$) for each interaction was derived using the ProteOn Manager software, using a 1:1 ratio. Alternatively, SPR experiments were conducted at 20 °C on a BIAcore 3000 instrument in 10 mM HEPES, pH 7.4, 150 mM NaCl supplemented with 0.5 % (w/v) bovine serum albumin. The analytes were captured on a CM5 sensor chip via amine-coupling. This was used to immobilise PE, mouse (m) CD1d-α-GalCer, I-A^b-CLIP, H2-D^b-NP_{366} and mMR1-5-OP-RU to a surface density of ~1000 response units. Serial dilutions from 200 to 0 µM of the 4D4 and 2C12 TCRs were injected over the immobilised proteins, notwithstanding the 2C12 TCR binding to mCD1d which owing to its extremely high affinity we used a maximum concentration of 5 µM. For the CD1d lipid specificity experiments, mCD1d-endo, mCD1d-α-GalCer and mCD1d-α-GlcADAG were immobilised on a sensor chip by biotin capture to ~3000 response units. Two-fold dilutions of soluble 4D4 TCR, or the NKT A11B8.2 and 2C12 TCRs, starting at 100, 200 and 5 µM respectively, were passed over the chip. SPR experiments were performed in experimental duplicate and in independent repeats except A11B8.2 ($n = 1$). The kinetic parameters calculated using the BIAevaluation program using 1:1 Langmuir binding model and plotted in GraphPad Prism software version 5.

Isothermal titration calorimetry

ITC experiments were carried out at 25 °C using a Microcal iTC200 instrument. Prior to the assay all samples were buffer exchanged into PBS pH 8. PE (200 µL in the cell) was titrated with 4D4 TCR in 2.49 µl aliquots of titrant (total of 43 µL) with an injection time of 10 seconds. In one experiment (shown) 4D4 TCR and PE were used at 660 µM and 17.73 µM, respectively. On a separate experiment TCR an PE were use at 352 µM and 18.49 µM, respectively. Data was normalised to heat variations due to the dilution of 4D4 TCR into buffer, or the dilution of buffer into PE, in the sample chamber. Data was analysed on the MicroCal ITC-Origin analysis software. The affinity constant (K_d), stoichiometry of binding (n), enthalpy (ΔH) and entropy (ΔS) for the binding reaction were estimated by the best fit of 200 interactions using the Microcal Origin 7 software for each experiment and then averaged.

Sedimentation velocity analytical ultracentrifugation

Prior to SV-AUC, each sample was buffer exchanged into TBS pH 8.0. The 4D4 TCR (10 µM) was mixed with non-conjugated PE (Prozyme, 1 µM) at a 10:1 molar ratio in an AUC analysis cuvette (400 µL). The total amount of protein was used at 0.8 mg/mL to ensure the absorbance at 280 nm was <1.5. Samples were analysed using an XL-I analytical ultracentrifuge (Beckman Coulter, Indianapolis, USA) equipped with an AnTi-60 rotor. Protein samples were loaded in the sample compartment of double-sector epon centrepieces, with buffer in the reference compartment. Radial absorbance data was acquired at 20 °C using a rotor speed of 72 400 g and a wavelength of 280 nm, with radial increments of 0.003 cm in continuous scanning mode. The sedimenting boundaries were fitted to a model that describes the sedimentation of a distribution of sedimentation coefficients with no assumption of heterogeneity (c(s)) using the program SEDFIT[70]. Data were fitted using a regularisation parameter of p = 0.95, floating frictional ratios, and 100 sedimentation coefficient increments in the range of 0–20 S.

Crystallisation, structure determination and refinement

Hexagonal crystals of the phycoerythrin protein grew in 0.1 M sodium acetate pH 4.5, 1.2 M ammonium sulfate, 4 % (w/v) benzamidine hydrochloride. Crystals were flash-frozen in mother liquor

supplemented with 27.5% (v/v) glycerol, data were collected at the Australian Synchrotron MX2 beamline, Melbourne. Data were processed with the program iMosflm[71] and were scaled with the SCALA program of the CCP4 suite[72]. Crystals belonged to the R3 space group and diffracted to 2.0 Å resolution. Molecular replacement was carried out with the program Phenix PHASER[73] using the structure of R-phycoerythrin from *Gracilaria chilensis* (PDB code 1EYX[74]) as the search ensemble. Model refinement was performed with iterative rounds of optimisation with COOT[75] and Phenix REFINE[76] to yield final model R_{factor} and R_{free} values of 19.8 % and 25.1 %, respectively. The density for the phycoerythrobilin moieties was unambiguous. The refined phycoerythrin structure was utilised for the subsequent refinement of the TCR complex. Hexagonal crystals of the 4D4-phycoerythrin complex grew in 0.1 M sodium acetate pH 4.5, 1.2 M ammonium sulfate, 5 % (w/v) D-sorbitol. Crystals were flash-frozen in mother liquor supplemented with 30 % (v/v) glycerol, and data were collected and processed as above. Crystals belonged to the P622 space group and diffracted to 3.0 Å resolution. Molecular replacement was carried out using the structures of the *Mus musculus* αβ 5 c.c7 TCR (α-chain) and the A11B8.2 NKT TCR (β-chain) (PDB codes 3QJH[77] and 6MRA[31] respectively) as separate search ensembles, and iteratively refined as above to yield final R_{factor} and R_{free} values of 25.7% and 26.9%, respectively. Unit cell minimisation was conducted with the program ACHESYM[78]. All presentations of molecular graphics were created with PyMOL molecular visualization system (The PyMOL Molecular Graphics System, Version 1.5.0.4 Schrödinger, LLC.). Estimation and visualisation of the evolutionary conservation of the PE α-chain was conducted using multiple sequence alignments and visualised using the online Consurf server[79].

Reporting summary

Further information on research design is available in the Nature Portfolio Reporting Summary linked to this article.

Data availability

Crystal structures of the 4D4 TCR-Phycoerythrin complex and Phycoerythrin in this study have been deposited in the Protein Databank under accession codes 8U0Y and 8U0F, respectively. All remaining data are available within the article and associated files and upon reasonable request from the corresponding authors. Source data are provided in this paper.

Code availability

The link to the cluster analysis algorithm used in this study is available at GitHub repository link (https://github.com/PRNicovich/ClusDoC)[80].

References

1. La Gruta, N. L., Gras, S., Daley, S. R., Thomas, P. G. & Rossjohn, J. Understanding the drivers of MHC restriction of T cell receptors. *Nat. Rev. Immunol.* **18**, 467–478 (2018).
2. Rossjohn, J. et al. T cell antigen receptor recognition of antigen-presenting molecules. *Annu Rev Immunol.* **33**, 169–200 (2015).
3. Doherty, P. C. & Zinkernagel, R. M. A biological role for the major histocompatibility antigens. *Lancet* **1**, 1406–1409 (1975).
4. Birkinshaw, R. W. et al. alphabeta T cell antigen receptor recognition of CD1a presenting self lipid ligands. *Nat. Immunol.* **16**, 258–266 (2015).
5. Nicolai, S. et al. Human T cell response to CD1a and contact dermatitis allergens in botanical extracts and commercial skin care products. *Sci. Immunol.* **5**, eaax5430 (2020).
6. Wun, K. S. et al. T cell autoreactivity directed toward CD1c itself rather than toward carried self lipids. *Nat. Immunol.* **19**, 397–406 (2018).
7. Willcox, C. R. et al. Cytomegalovirus and tumor stress surveillance by binding of a human gammadelta T cell antigen receptor to endothelial protein C receptor. *Nat. Immunol.* **13**, 872–879 (2012).
8. Luoma, A. M. et al. Crystal structure of Vdelta1 T cell receptor in complex with CD1d-sulfatide shows MHC-like recognition of a self-lipid by human gammadelta T cells. *Immunity* **39**, 1032–1042 (2013).
9. Uldrich, A. P. et al. CD1d-lipid antigen recognition by the gamma-delta TCR. *Nat. Immunol.* **14**, 1137–1145 (2013).
10. Almeida, C. F. et al. Benzofuran sulfonates and small self-lipid antigens activate type II NKT cells via CD1d. *Proc. Natl Acad. Sci. USA* **118**, e2104420118 (2021).
11. Crowley, M. P. et al. A population of murine gammadelta T cells that recognize an inducible MHC class Ib molecule. *Science* **287**, 314–316 (2000).
12. Le Nours, J. et al. A class of gammadelta T cell receptors recognize the underside of the antigen-presenting molecule MR1. *Science* **366**, 1522–1527 (2019).
13. Adams, E. J., Chien, Y. H. & Garcia, K. C. Structure of a gammadelta T cell receptor in complex with the nonclassical MHC T22. *Science* **308**, 227–231 (2005).
14. Adams, E. J., Strop, P., Shin, S., Chien, Y. H. & Garcia, K. C. An autonomous CDR3delta is sufficient for recognition of the non-classical MHC class I molecules T10 and T22 by gammadelta T cells. *Nat. Immunol.* **9**, 777–784 (2008).
15. Shin, S. et al. Antigen recognition determinants of gammadelta T cell receptors. *Science* **308**, 252–255 (2005).
16. Wu, J., Groh, V. & Spies, T. T cell antigen receptor engagement and specificity in the recognition of stress-inducible MHC class I-related chains by human epithelial gamma delta T cells. *J. Immunol.* **169**, 1236–1240 (2002).
17. Xu, B. et al. Crystal structure of a gammadelta T-cell receptor specific for the human MHC class I homolog MICA. *Proc. Natl Acad. Sci. USA* **108**, 2414–2419 (2011).
18. Reijneveld, J. F. et al. Human gammadelta T cells recognize CD1b by two distinct mechanisms. *Proc. Natl Acad. Sci. USA* **117**, 22944–22952 (2020).
19. Rice, M. T. et al. Recognition of the antigen-presenting molecule MR1 by a Vδ3 + γδ T cell receptor. *Proc. Natl Acad. Sci. USA* **118**, e2110288118 (2021).
20. Sandstrom, A. et al. The intracellular B30.2 domain of butyrophilin 3A1 binds phosphoantigens to mediate activation of human Vgamma9Vdelta2 T cells. *Immunity* **40**, 490–500 (2014).
21. Willcox, C. R. et al. Butyrophilin-like 3 Directly Binds a Human Vgamma4(+) T Cell Receptor Using a Modality Distinct from Clonally-Restricted Antigen. *Immunity* **51**, 813–825 e814 (2019).
22. Melandri, D. et al. The gammadeltaTCR combines innate immunity with adaptive immunity by utilizing spatially distinct regions for agonist selection and antigen responsiveness. *Nat. Immunol.* **19**, 1352–1365 (2018).
23. Rigau, M. et al. Butyrophilin 2A1 is essential for phosphoantigen reactivity by gammadelta T cells. *Science* **367**, eaay5516 (2020).
24. Uldrich, A. P., Rigau, M. & Godfrey, D. I. Immune recognition of phosphoantigen-butyrophilin molecular complexes by gamma-delta T cells. *Immunol. Rev.* **298**, 74–83 (2020).
25. Gully, B. S., Rossjohn, J. & Davey, M. S. Our evolving understanding of the role of the gammadelta T cell receptor in gammadelta T cell mediated immunity. *Biochem Soc. Trans.* **49**, 1985–1995 (2021).
26. Zeng, X. et al. gammadelta T cells recognize a microbial encoded B cell antigen to initiate a rapid antigen-specific interleukin-17 response. *Immunity* **37**, 524–534 (2012).
27. Van Laethem, F. et al. Deletion of CD4 and CD8 coreceptors permits generation of alphabeta T cells that recognize antigens independently of the MHC. *Immunity* **27**, 735–750 (2007).
28. Tikhonova, A. N. et al. alphabeta T cell receptors that do not undergo major histocompatibility complex-specific thymic selection possess antibody-like recognition specificities. *Immunity* **36**, 79–91 (2012).

29. Van Laethem, F. et al. Novel MHC-Independent alphabetaTCRs Specific for CD48, CD102, and CD155 Self-Proteins and Their Selection in the Thymus. *Front Immunol.* **11**, 1216 (2020).
30. Lu, J. et al. Structure of MHC-Independent TCRs and Their Recognition of Native Antigen CD155. *J. Immunol.* **204**, 3351–3359 (2020).
31. Almeida, C. F. et al. Distinct CD1d docking strategies exhibited by diverse Type II NKT cell receptors. *Nat. Commun.* **10**, 5242 (2019).
32. Pellicci, D. G. et al. Differential recognition of CD1d-alpha-galactosyl ceramide by the V beta 8.2 and V beta 7 semi-invariant NKT T cell receptors. *Immunity* **31**, 47–59 (2009).
33. Cardell, S. et al. CD1-restricted CD4 + T cells in major histocompatibility complex class II-deficient mice. *J. Exp. Med.* **182**, 993–1004 (1995).
34. Pape, K. A., Taylor, J. J., Maul, R. W., Gearhart, P. J. & Jenkins, M. K. Different B cell populations mediate early and late memory during an endogenous immune response. *Science* **331**, 1203–1207 (2011).
35. Wu, C. J., Karttunen, J. T., Chin, D. H., Sen, D. & Gilbert, W. Murine memory B cells are multi-isotype expressors. *Immunology* **72**, 48–55 (1991).
36. Klotz, A. V. & Glazer, A. N. Characterization of the bilin attachment sites in R-phycoerythrin. *J. Biol. Chem.* **260**, 4856–4863 (1985).
37. Tatituri, R. V. et al. Recognition of microbial and mammalian phospholipid antigens by NKT cells with diverse TCRs. *Proc. Natl Acad. Sci. USA* **110**, 1827–1832 (2013).
38. Orta-Ramirez, A. & Smith, D. M. Thermal inactivation of pathogens and verification of adequate cooking in meat and poultry products. *Adv. food Nutr. Res.* **44**, 147–194 (2002).
39. Bell, J. & Gray, D. Antigen-capturing cells can masquerade as memory B cells. *J. Exp. Med.* **197**, 1233–1244 (2003).
40. Takizawa, F., Kinet, J. P. & Adamczewski, M. Binding of phycoerythrin and its conjugates to murine low affinity receptors for immunoglobulin G. *J. Immunol. Methods* **162**, 269–272 (1993).
41. van Vugt, M. J. & van den Herik-Oudijk, I. E. van de Winkle JG. Binding of PE-CY5 conjugates to the human high-affinity receptor for IgG (CD64). *Blood* **88**, 2358–2361 (1996).
42. Cassatella, M. A. et al. Interferon-gamma transcriptionally modulates the expression of the genes for the high affinity IgG-Fc receptor and the 47-kDa cytosolic component of NADPH oxidase in human polymorphonuclear leukocytes. *J. Biol. Chem.* **266**, 22079–22082 (1991).
43. Haig, N. A. et al. Identification of self-lipids presented by CD1c and CD1d proteins. *J. Biol. Chem.* **286**, 37692–37701 (2011).
44. Garcia, K. C., Radu, C. G., Ho, J., Ober, R. J. & Ward, E. S. Kinetics and thermodynamics of T cell receptor- autoantigen interactions in murine experimental autoimmune encephalomyelitis. *Proc. Natl Acad. Sci. USA* **98**, 6818–6823 (2001).
45. van der Merwe, P. A. & Davis, S. J. Molecular interactions mediating T cell antigen recognition. *Annu. Rev. Immunol.* **21**, 659–684 (2003).
46. Glazer, A. N. Light harvesting by phycobilisomes. *Annu. Rev. Biophys. Biophys. Chem.* **14**, 47–77 (1985).
47. Glazer, A. N. Phycobiliproteins. *Methods Enzymol.* **167**, 291–303 (1988).
48. Glazer, A. N. Light guides. Directional energy transfer in a photosynthetic antenna. *J. Biol. Chem.* **264**, 1–4 (1989).
49. Holst, J. et al. Generation of T-cell receptor retrogenic mice. *Nat. Protoc.* **1**, 406–417 (2006).
50. Dash, P. et al. Paired analysis of TCRalpha and TCRbeta chains at the single-cell level in mice. *J. Clin. Investig.* **121**, 288–295 (2011).
51. Singh, N. K. et al. An engineered T cell receptor variant realizes the limits of functional binding modes. *Biochemistry* **59**, 4163–4175 (2020).
52. Cotton, R. N. et al. Human skin is colonized by T cells that recognize CD1a independently of lipid. *J. Clin. Investig.* **131**, e140706 (2021).
53. Cotton, R. N. et al. CD1a selectively captures endogenous cellular lipids that broadly block T cell response. *J. Exp. Med.* **218**, e20202699 (2021).
54. Cotton, R. N., Shahine, A., Rossjohn, J. & Moody, D. B. Lipids hide or step aside for CD1-autoreactive T cell receptors. *Curr. Opin. Immunol.* **52**, 93–99 (2018).
55. Hanada, K., Wang, Q. J., Inozume, T. & Yang, J. C. Molecular identification of an MHC-independent ligand recognized by a human {alpha}/{beta} T-cell receptor. *Blood* **117**, 4816–4825 (2011).
56. Stadinski, B. D. et al. Hydrophobic CDR3 residues promote the development of self-reactive T cells. *Nat. Immunol.* **17**, 946–955 (2016).
57. Zeng, X. et al. γδ T cells recognize a microbial encoded B cell antigen to initiate a rapid antigen-specific interleukin-17 response. *Immunity* **37**, 524–534 (2012).
58. Nombela, I. & Ortega-Villaizan, M. D. M. Nucleated red blood cells: Immune cell mediators of the antiviral response. *PLoS Pathog.* **14**, e1006910 (2018).
59. Pellicci, D. G., Koay, H. F. & Berzins, S. P. Thymic development of unconventional T cells: how NKT cells, MAIT cells and gammadelta T cells emerge. *Nat. Rev. Immunol.* **20**, 756–770 (2020).
60. Cian, R. E., Drago, S. R., de Medina, F. S. & Martinez-Augustin, O. Proteins and carbohydrates from red Seaweeds: evidence for beneficial effects on gut function and microbiota. *Mar. Drugs* **13**, 5358–5383 (2015).
61. Sekar, S. & Chandramohan, M. Phycobiliproteins as a commodity: trends in applied research, patents and commercialisation. *J. Appl Phycol. Commer.* **20**, 113–136 (2008).
62. Szymczak, A. L. et al. Correction of multi-gene deficiency in vivo using a single 'self-cleaving' 2 A peptide-based retroviral vector. *Nat. Biotechnol.* **22**, 589–594 (2004).
63. Holst, J., Vignali, K. M., Burton, A. R. & Vignali, D. A. Rapid analysis of T-cell selection in vivo using T cell-receptor retrogenic mice. *Nat. Methods* **3**, 191–197 (2006).
64. Aricescu, A. R. et al. Eukaryotic expression: developments for structural proteomics. *Acta Crystallogr D. Biol. Crystallogr* **62**, 1114–1124 (2006).
65. Burugupalli, S. et al. Glucuronosyl and α-glucosyl diacylglycerides, natural killer T cell-activating lipids from bacteria and fungi. *Chem. Sci.* **11**, 2161–2168 (2020).
66. Helft, J. et al. GM-CSF mouse bone marrow cultures comprise a heterogeneous population of CD11c(+)MHCII(+) macrophages and dendritic cells. *Immunity* **42**, 1197–1211 (2015).
67. Pageon, S. V. et al. Functional role of T-cell receptor nanoclusters in signal initiation and antigen discrimination. *Proc. Natl Acad. Sci.* **113**, E5454–E5463 (2016).
68. Kjer-Nielsen, L. et al. A structural basis for selection and cross-species reactivity of the semi-invariant NKT cell receptor in CD1d/glycolipid recognition. *J. Exp. Med.* **203**, 661–673 (2006).
69. Arndt, C., Koristka, S., Bartsch, H. & Bachmann, M. Native polyacrylamide gels. *Methods Mol. Biol.* **869**, 49–53 (2012).
70. Schuck, P. Size-distribution analysis of macromolecules by sedimentation velocity ultracentrifugation and lamm equation modeling. *Biophys. J.* **78**, 1606–1619 (2000).
71. Battye, T. G. G., Kontogiannis, L., Johnson, O., Powell, H. R. & Leslie, A. G. W. iMOSFLM: a new graphical interface for diffraction-image processing with MOSFLM. *Acta Crystallogr. Sect. D. Biol. Crystallogr.* **67**, 271–281 (2011).
72. Winn, M. D. et al. Overview of the CCP4 suite and current developments. *Acta Crystallogr. Sect. D. Biol. Crystallogr.* **67**, 235–242 (2011).
73. McCoy, A. J. et al. Phaser crystallographic software. *J. Appl. Crystallogr.* **40**, 658–674 (2007).
74. Contreras-Martel, C. et al. Crystallization and 2.2 A resolution structure of R-phycoerythrin from Gracilaria chilensis: a case of

perfect hemihedral twinning. *Acta Crystallogr D. Biol. Crystallogr* **57**, 52–60 (2001).
75. Emsley, P., Lohkamp, B., Scott, W. G. & Cowtan, K. Features and development of Coot. *Acta Crystallogr. Sect. D Biol. Crystallogr.* **66**, 486–501 (2010).
76. Afonine, P. V. et al. Towards automated crystallographic structure refinement with phenix.refine. *Acta Crystallogr. Sect. D* **68**, 352–367 (2012).
77. Newell, E. W. et al. Structural basis of specificity and cross-reactivity in T cell receptors specific for cytochrome c-I-E(k). *J. Immunol.* **186**, 5823 (2011).
78. Kowiel, M., Jaskolski, M. & Dauter, Z. ACHESYM: an algorithm and server for standardized placement of macromolecular models in the unit cell. *Acta Crystallogr. Sect. D Biol. Crystallogr.* **70**, 3290–3298 (2014).
79. Ashkenazy, H. et al. ConSurf 2016: an improved methodology to estimate and visualize evolutionary conservation in macromolecules. *Nucleic Acids Res.* **44**, W344–W350 (2016).
80. Pageon, S. V., Nicovich, P. R., Mollazade, M., Tabarin, T. & Gaus, K. Clus-DoC: a combined cluster detection and colocalization analysis for single-molecule localization microscopy data. *Mol. Biol. Cell* **27**, 3627–3636 (2016).
81. Chan, K. F. et al. Divergent T-cell receptor recognition modes of a HLA-I restricted extended tumour-associated peptide. *Nat. Commun.* **9**, 1026 (2018).
82. Kjer-Nielsen, L. et al. MR1 presents microbial vitamin B metabolites to MAIT cells. *Nature* **491**, 717–723 (2012).
83. Li, P. et al. Complex structure of the activating immunoreceptor NKG2D and its MHC class I–like ligand MICA. *Nat. Immunol.* **2**, 443–451 (2001).
84. Rudolph, M. G., Wingren, C., Crowley, M. P., Chien, Y.-H. & Wilson, I. A. Combined pseudo-merohedral twinning, non-crystallographic symmetry and pseudo-translation in a monoclinic crystal form of the [gamma][delta] T-cell ligand T10. *Acta Crystallogr. Sect. D.* **60**, 656–664 (2004).
85. Wingren, C., Crowley Michael, P., Degano, M., Chien, Y.-H. & Wilson Ian, A. Crystal structure of a γδ T cell receptor ligand T22: a truncated MHC-like fold. *Science* **287**, 310–314 (2000).
86. Berry, R. et al. Targeting of a natural killer cell receptor family by a viral immunoevasin. *Nat. Immunol.* **14**, 699–705 (2013).
87. Martin, W. L., West, A. P. Jr, Gan, L. & Bjorkman, P. J. Crystal Structure at 2.8 Å of an FcRn/Heterodimeric Fc Complex: Mechanism of pH-Dependent Binding. *Mol. Cell* **7**, 867–877 (2001).
88. Lebrón, J. A. et al. Crystal Structure of the Hemochromatosis Protein HFE and Characterization of Its Interaction with Transferrin Receptor. *Cell* **93**, 111–123 (1998).
89. Sen, U. et al. Crystal Structures of HbA2 and HbE and Modeling of Hemoglobin δ4: Interpretation of the Thermal Stability and the Antisickling Effect of HbA2 and Identification of the Ferrocyanide Binding Site in Hb. *Biochemistry* **43**, 12477–12488 (2004).
90. Pesce, A. et al. Human brain neuroglobin structure reveals a distinct mode of controlling oxygen affinity. *Structure* **11**, 1087–1095 (2003).
91. Teh, A.-H. et al. Hell's Gate globin I: An acid and thermostable bacterial hemoglobin resembling mammalian neuroglobin. *FEBS Lett.* **585**, 3250–3258 (2011).

Acknowledgements

We are grateful to Dr. Paul Savage (Brigham Young University, UT, USA) and Prof Spencer Williams (Bio21, University of Melbourne, Australia) for providing α-GalCer analog PBS44 and α-GlcADAG, respectively, used for the production of CD1d-tetramers. We thank the staff at the Australian Synchrotron for assistance with data collection, the staff at the Monash Macromolecular crystallisation facility, the staff at the Monash Animal Research platform and the staff from the University of Melbourne flow cytometry facilities. This research was undertaken on the MX1 and MX2 beamlines at the Australian Synchrotron, part of ANSTO, and at the Protein Interactions Facility at the Melbourne Protein Characterisation (MPC), located within the Bio21 Institute, Melbourne. We would like to thank Senthil Arumugam at Monash Biomedicine Discovery Institute for providing relevant training and access to the super-resolution microscope required to perform single-molecule imaging. We thank Marcin Ciula, Thomas Fulford, and Calvin Xu for their technical assistance. This work was supported by the Australian Research Council (ARC DP170104386), the National Health and Medical Research Council of Australia (NHMRC; 1013667 and 1016629), CFA was also supported by a Fundação para a Ciência e a Tecnologia (FCT; SFRH/BD/74906/2010) and NHMRC (2029256); APU was supported by a Future Fellowship (FT140100278). JR and DIG are supported by NHMRC Investigator Grants (2008981, 2008913). DBM is supported by the NIH (AR048632).

Author contributions

C.F.A. and B.S.G. are joint 1st authors and were major contributors to data generation and analysis. L.K., C.M.J., T.T.N., S.D.G., M.T.R., R.B., N.A.G., Y.F.M., J.F.R., D.B.M., I.V.R., N.L.L.G., A.P.U. contributed to data generation, analysis, and interpretation. A.P.U., J.R., and D.I.G. conceived the study and carried out project oversight and direction. C.F.A., B.S.G., A.P.U., J.R., and D.I.G. co-wrote the paper.

Competing interests

The authors declare no competing interests.

Additional information

Supplementary information The online version contains supplementary material available at https://doi.org/10.1038/s41467-024-51897-3.

Correspondence and requests for materials should be addressed to Adam P. Uldrich, Jamie Rossjohn or Dale I. Godfrey.